FIG. 5. Proposed structure and biosynthetic genes of GPL-S8 (serovar 8-specific GPL). Me, methyl.

region, suggesting that focusing on this region might provide clues for elucidating the characteristics of other ssGPLs whose biosynthesis is still not known.

It has been reported previously that the *gtfTB* gene in *M. avium* strains 104 and A5 was not likely to be associated with GPL biosynthesis because its ancestral homologue, Rv1516c (61% identity with the GtfTB gene), was the gene of *M. tuberculosis*, which produces no GPLs (28). Thus, it was interesting that *gtfTB* encodes a glycosyltransferase that does participate in GPL biosynthesis in which a Glc residue is transferred to serovar 1-specific GPL, yielding the serovar 8-specific GPL. *M. avium* strains 104 and A5 synthesize serovar 1-specific GPL as a final product and intermediate, respectively, while it has been recognized that neither of these strains produces serovar 8-specific GPL in spite of the presence of *gtfTB* in the GPL biosynthetic gene cluster (28). These observations raised the possibility that the transcription of *gtfTB* is inefficient in both strains due to the upstream sequences. Actually, in *M. avium* strain 104, a transposase sequence was observed upstream of *gtfTB*, indicating that this strain might be deficient in glucosylation, and consequently a serovar 1-specific GPL-producing strain is obtained (28). On the other hand, it has been shown that the biosynthetic gene cluster for serovar 7-specific GPL in *M. intracellulare* strain ATCC 35847 contains a putative glycosyltransferase gene which encodes amino acid sequences that are similar to the amino acid sequences encoded by *gtfTB* (59% identity) (18). Structural analysis of sugar moieties in serovar 7-specific GPL indicated that this GtfTB homologue may serve as a glycosyltransferase during formation of the terminal amidohexose residue that structurally resembles Glc (18).

The deduced amino acid sequences encoded by ORF3 and ORF4 showed that these genes putatively encode polysaccharide pyruvyltransferase and *O*-methyltransferase, respectively. Expression of ORF3 and ORF4 together with *gtfTB* led to structural alterations in which Glc was modified with both 4,6-*O*-(1-carboxyethylidene) and 3-*O*-methyl groups. Based on these observations, it is strongly suggested that ORF3 is associated with the formation of the 4,6-*O*-(1-carboxyethylidene) group that is synonymous with the cyclic pyruvate ketal and that ORF4 is associated with the 3-*O*-methylation of the Glc

residue (Fig. 5). In mycobacteria, homologues of ORF3 and ORF4 were found only in *M. smegmatis*, as MSMEG_4736 (for ORF3), MSMEG_4737 (for ORF3), and MSMEG_4739 (for ORF4). *M. smegmatis* also produces glycolipids containing 4,6-*O*-(1-carboxyethylidene)-3-*O*-methyl-Glc as a sugar moiety (25, 34), which suggests that both homologues participate in the synthesis of these glycolipids. Sugar residues with a 4,6-*O*-(1-carboxyethylidene) group substitution have been found in carbohydrates such as extracellular polysaccharide and N-linked glycan, which are produced by some bacteria and yeasts (1, 15, 20, 22, 26). It has been shown that an increase in 4,6-*O*-(1-carboxyethylidene)-containing sugar residues leads to enhanced viscosity of extracellular polysaccharide from *Xanthomonas* sp., which alters the cell surface properties related to cellular attachment and protection from environmental stress (10). Accordingly, in terms of the properties of serovar 8-specific GPL, the presence of the 4,6-*O*-(1-carboxyethylidene) group might influence the pathogenicity of MAC serovar 8.

With regard to the antibody reactivity, it is unclear whether serovar 8-specific antibodies react with GPL-S8 because there are minor structural differences in the methylated positions of fatty acids and the terminal Rha residue linked to the tetrapeptide between GPL-S8 and serovar 8-specific GPL of MAC. Evaluation of the antibody response to GPL-S8 using serovar 8-specific antibodies would facilitate understanding the immunoreactivity mediated by ssGPLs.

In this study, we proved that *gtfTB* and adjacent genes in the GPL biosynthetic gene cluster in MAC serovar 8 strain are responsible for the formation of a unique glucose residue in serovar 8-specific GPL (Fig. 5). In particular, *gtfTB* encodes the glucosyltransferase that plays a critical role in the pathway leading from serovar 1-specific GPL to serovar 8-specific GPL. Through further study, including generation of *gtfTB* knockout mutants of MAC serovar 8 strains, results relevant to the biosynthesis of serovar 8-specific GPL might help clarify the biological function of ssGPLs and their role in the host-pathogen relationships of MAC.

REFERENCES

1. **Aman, P., M. McNeil, L.-E. Franzen, A. G. Darvill, and P. Albersheim.** 1981. Structural elucidation, using HPLC-MS and GLC-MS, of the acidic exopolysaccharide secreted by *Rhizobium meliloti* strain Rm1021. Carbohydr. Res. **95:**263–282.
2. **Aspinall, G. O., D. Chatterjee, and P. J. Brennan.** 1995. The variable surface glycolipids of mycobacteria: structures, synthesis of epitopes, and biological properties. Adv. Carbohydr. Chem. Biochem. **51:**169–242.
3. **Barrow, W. W., T. L. Davis, E. L. Wright, V. Labrousse, M. Bachelet, and N. Rastogi.** 1995. Immunomodulatory spectrum of lipids associated with *Mycobacterium avium* serovar 8. Infect. Immun. **63:**126–133.
4. **Belisle, J. T., K. Klaczkiewicz, P. J. Brennan, W. R. Jacobs, Jr., and J. M. Inamine.** 1993. Rough morphological variants of *Mycobacterium avium*. Characterization of genomic deletions resulting in the loss of glycopeptidolipid expression. J. Biol. Chem. **268:**10517–10523.
5. **Bhatnagar, S., and J. S. Schorey.** 2007. Exosomes released from infected macrophages contain *Mycobacterium avium* glycopeptidolipids and are proinflammatory. J. Biol. Chem. **282:**25779–25789.
6. **Bjorndal, H., C. G. Hellerqvist, B. Lindberg, and S. Svensson.** 1970. Gas-liquid chromatography and mass spectrometry in methylation analysis of polysaccharides. Angew. Chem. Int. Ed. Engl. **9:**610–619.

7. Brennan, P. J., G. O. Aspinall, and J. E. Shin. 1981. Structure of the specific oligosaccharides from the glycopeptidolipid antigens of serovars in the *Mycobacterium avium-Mycobacterium intracellulare-Mycobacterium scrofulaceum* complex. J. Biol. Chem. **256**:6817–6822.

8. Brennan, P. J., H. Mayer, G. O. Aspinall, and J. E. Nam Shin. 1981. Structures of the glycopeptidolipid antigens from serovars in the *Mycobacterium avium/Mycobacterium intracellulare/Mycobacterium scrofulaceum* sero-complex. Eur. J. Biochem. **115**:7–15.

9. Brennan, P. J., and H. Nikaido. 1995. The envelope of mycobacteria. Annu. Rev. Biochem. **64**:29–63.

10. Casas, J. A., V. E. Santos, and F. Garcia-Ochoa. 2000. Xanthan gum production under several operational conditions: molecular structure and rheological properties. Enzyme Microb. Technol. **26**:282–291.

11. Chatterjee, D., and K. H. Khoo. 2001. The surface glycopeptidolipids of mycobacteria: structures and biological properties. Cell. Mol. Life Sci. **58**:2018–2042.

12. Ciucanu, I., and F. Kerek. 1984. A simple and rapid method for the permethylation of carbohydrates. Carbohydr. Res. **131**:209–217.

13. Daffe, M., and P. Draper. 1998. The envelope layers of mycobacteria with reference to their pathogenicity. Adv. Microb. Physiol. **39**:131–203.

14. Daffe, M., M. A. Laneelle, and G. Puzo. 1983. Structural elucidation by field desorption and electron-impact mass spectrometry of the C-mycosides isolated from *Mycobacterium smegmatis*. Biochim. Biophys. Acta **751**:439–443.

15. D'Haeze, W., J. Glushka, R. De Rycke, M. Holsters, and R. W. Carlson. 2004. Structural characterization of extracellular polysaccharides of *Azorhizobium caulinodans* and importance for nodule initiation on *Sesbania rostrata*. Mol. Microbiol. **52**:485–500.

16. Eckstein, T. M., J. T. Belisle, and J. M. Inamine. 2003. Proposed pathway for the biosynthesis of serovar-specific glycopeptidolipids in *Mycobacterium avium* serovar 2. Microbiology **149**:2797–2807.

17. Eckstein, T. M., F. S. Silbaq, D. Chatterjee, N. J. Kelly, P. J. Brennan, and J. T. Belisle. 1998. Identification and recombinant expression of a *Mycobacterium avium* rhamnosyltransferase gene (*rtfA*) involved in glycopeptidolipid biosynthesis. J. Bacteriol. **180**:5567–5573.

18. Fujiwara, N., N. Nakata, S. Maeda, T. Naka, M. Doe, I. Yano, and K. Kobayashi. 2007. Structural characterization of a specific glycopeptidolipid containing a novel *N*-acyl-deoxy sugar from *Mycobacterium intracellulare* serotype 7 and genetic analysis of its glycosylation pathway. J. Bacteriol. **189**:1099–1108.

19. Fujiwara, N., N. Nakata, T. Naka, I. Yano, M. Doe, D. Chatterjee, M. McNeil, P. J. Brennan, K. Kobayashi, M. Makino, S. Matsumoto, H. Ogura, and S. Maeda. 2008. Structural analysis and biosynthesis gene cluster of an antigenic glycopeptidolipid from *Mycobacterium intracellulare*. J. Bacteriol. **190**:3613–3621.

20. Gemmill, T. R., and R. B. Trimble. 1996. *Schizosaccharomyces pombe* produces novel pyruvate-containing N-linked oligosaccharides. J. Biol. Chem. **271**:25945–25949.

21. Horgen, L., E. L. Barrow, W. W. Barrow, and N. Rastogi. 2000. Exposure of human peripheral blood mononuclear cells to total lipids and serovar-specific glycopeptidolipids from *Mycobacterium avium* serovars 4 and 8 results in inhibition of TH1-type responses. Microb. Pathog. **29**:9–16.

22. Jansson, P. E., L. Kenne, and B. Lindberg. 1975. Structure of extracellular polysaccharide from *Xanthomonas campestris*. Carbohydr. Res. **45**:275–282.

23. Jeevarajah, D., J. H. Patterson, M. J. McConville, and H. Billman-Jacobe. 2002. Modification of glycopeptidolipids by an *O*-methyltransferase of *Mycobacterium smegmatis*. Microbiology **148**:3079–3087.

24. Julander, I., S. Hoffner, B. Petrini, and L. Ostlund. 1996. Multiple serovars of *Mycobacterium avium* complex in patients with AIDS. APMIS **104**:318–320.

25. Kamisango, K., S. Saadat, A. Dell, and C. E. Ballou. 1985. Pyruvylated glycolipids from *Mycobacterium smegmatis*. Nature and location of the lipid components. J. Biol. Chem. **260**:4117–4121.

26. Kojima, N., S. Kaya, Y. Araki, and E. Ito. 1988. Pyruvic-acid-containing polysaccharide in the cell wall of *Bacillus polymyxa* AHU 1385. Eur. J. Biochem. **174**:255–260.

27. Krzywinska, E., S. Bhatnagar, L. Sweet, D. Chatterjee, and J. S. Schorey. 2005. *Mycobacterium avium* 104 deleted of the methyltransferase D gene by allelic replacement lacks serotype-specific glycopeptidolipids and shows attenuated virulence in mice. Mol. Microbiol. **56**:1262–1273.

28. Krzywinska, E., and J. S. Schorey. 2003. Characterization of genetic differences between *Mycobacterium avium* subsp. *avium* strains of diverse virulence with a focus on the glycopeptidolipid biosynthesis cluster. Vet. Microbiol. **91**:249–264.

29. Li, Z., G. H. Bai, C. F. von Reyn, P. Marino, M. J. Brennan, N. Gine, and S. L. Morris. 1996. Rapid detection of *Mycobacterium avium* in stool samples from AIDS patients by immunomagnetic PCR. J. Clin. Microbiol. **34**:1903–1907.

30. Miyamoto, Y., T. Mukai, Y. Maeda, N. Nakata, M. Kai, T. Naka, I. Yano, and M. Makino. 2007. Characterization of the fucosylation pathway in the biosynthesis of glycopeptidolipids from *Mycobacterium avium* complex. J. Bacteriol. **189**:5515–5522.

31. Miyamoto, Y., T. Mukai, N. Nakata, Y. Maeda, M. Kai, T. Naka, I. Yano, and M. Makino. 2006. Identification and characterization of the genes involved in glycosylation pathways of mycobacterial glycopeptidolipid biosynthesis. J. Bacteriol. **188**:86–95.

32. Miyamoto, Y., T. Mukai, F. Takeshita, N. Nakata, Y. Maeda, M. Kai, and M. Makino. 2004. Aggregation of mycobacteria caused by disruption of fibronectin-attachment protein-encoding gene. FEMS Microbiol. Lett. **236**:227–234.

33. Patterson, J. H., M. J. McConville, R. E. Haites, R. L. Coppel, and H. Billman-Jacobe. 2000. Identification of a methyltransferase from *Mycobacterium smegmatis* involved in glycopeptidolipid synthesis. J. Biol. Chem. **275**:24900–24906.

34. Saadat, S., and C. E. Ballou. 1983. Pyruvylated glycolipids from *Mycobacterium smegmatis*. Structures of two oligosaccharide components. J. Biol. Chem. **258**:1813–1818.

35. Snapper, S. B., R. E. Melton, S. Mustafa, T. Kieser, and W. R. Jacobs, Jr. 1990. Isolation and characterization of efficient plasmid transformation mutants of *Mycobacterium smegmatis*. Mol. Microbiol. **4**:1911–1919.

36. Stover, C. K., V. F. de la Cruz, T. R. Fuerst, J. E. Burlein, L. A. Benson, L. T. Bennett, G. P. Bansal, J. F. Young, M. H. Lee, G. F. Hatfull, S. B. Snapper, R. G. Barletta, W. R. Jacobs, Jr., and B. R. Bloom. 1991. New use of BCG for recombinant vaccines. Nature **351**:456–460.

37. Sweet, L., and J. S. Schorey. 2006. Glycopeptidolipids from *Mycobacterium avium* promote macrophage activation in a TLR2- and MyD88-dependent manner. J. Leukoc. Biol. **80**:415–423.

38. Tassell, S. K., M. Pourshafie, E. L. Wright, M. G. Richmond, and W. W. Barrow. 1992. Modified lymphocyte response to mitogens induced by the lipopeptide fragment derived from *Mycobacterium avium* serovar-specific glycopeptidolipids. Infect. Immun. **60**:706–711.

39. Tsang, A. Y., J. C. Denner, P. J. Brennan, and J. K. McClatchy. 1992. Clinical and epidemiological importance of typing of *Mycobacterium avium* complex isolates. J. Clin. Microbiol. **30**:479–484.

40. Vergne, I., and M. Daffe. 1998. Interaction of mycobacterial glycolipids with host cells. Front. Biosci. **3**:d865–876.

41. Yakrus, M. A., and R. C. Good. 1990. Geographic distribution, frequency, and specimen source of *Mycobacterium avium* complex serotypes isolated from patients with acquired immunodeficiency syndrome. J. Clin. Microbiol. **28**:926–929.

The cellular niche of *Listeria monocytogenes* infection changes rapidly in the spleen

Taiki Aoshi[1], Javier A. Carrero[1], Vjollca Konjufca[1], Yukio Koide[2], Emil R. Unanue[1] and Mark J. Miller[1]

[1] Department of Pathology and Immunology, Washington University School of Medicine, St. Louis, MO, USA

[2] Department of Infectious Diseases, Hamamatsu University School of Medicine, Hamamatsu, Shizuoka, Japan

The spleen is an important organ for the host response to systemic bacterial infections. Many cell types and cell surface receptors have been shown to play role in the capture and control of bacteria, yet these are often studied individually and a coherent picture has yet to emerge of how various phagocytes collaborate to control bacterial infection. We analyzed the cellular distribution of *Listeria monocytogenes* (LM) *in situ* during the early phase of infection. Using an immunohistochemistry approach, five distinct phagocyte populations contained LM after i.v. challenge and accounted for roughly all bacterial signal in tissue sections. Our analysis showed that LM was initially captured by a wide range of phagocytes in the marginal zone, where the growth of LM appeared to be controlled. The cellular distribution of LM within phagocyte populations changed rapidly during the first few hours, decreasing in marginal zone macrophages and transiently increasing in CD11c^{+} DC. After 4–6 h LM was transported to the periarteriolar lymphoid sheath where the infective foci developed and LM grew exponentially.

Supporting Information available online

Introduction

The spleen is an important site for host responses to bacterial infection [1, 2]. Within the spleen, bacteria may encounter various tissue resident phagocytes including macrophages, DC, and neutrophils [3, 4]. Marginal zone macrophages (MZM) are positioned along the outer layer of the marginal sinus where they have direct access to bacteria entering the spleen from the circulation. These macrophages express MARCO (macrophage receptor with collagenous structure), a type-1 scavenger receptor,

related to the SR-A family of receptors [5], which recognizes bacterial cell-wall-associated polyanions [6]. MZM also express the C-type lectin, SIGN-R1. SIGN-R1 binds dextran [7] and facilitates the capture of polysaccharide antigens on bacteria such as *Streptococcus pneumoniae* [8]. A separate class of MZM, the metallophilic MZM (MMM), localize between the inner marginal sinus and the B-cell follicle [9]. These cells recognize sialic acid and LPS from *Neiseria meningitidis* [10] through Siglec-1 (sialic-acid-binding-Ig-like-lectin 1) [11, 12]. MMM have also been shown to produce interferon during Herpes simplex virus infection [13], but their role in bacterial infection is unclear, although it was reported that they produce CCL2 [14].

Neutrophils play a crucial role in controlling bacterial infection [15–19]. They are present in the marginal zone (MZ) and

Correspondence: Dr. Mark J. Miller
e-mail: miller@pathology.wustl.edu

red pulp (RP) of the spleen and therefore have access to circulating bacteria and bacteria released from infected splenocytes. Also within the MZ of the spleen resides a population of DC recognized with the antibody 33D1 [20], which have been shown to efficiently present antigens to CD4^{+} T cells [21]. The location of these cells in the MZ suggests that they may participate in the capture of bacteria in the circulation. Macrophages are also present in the RP [22]. These macrophages are F4/80[+] and primarily serve to remove dying red blood cells and other debris from the circulation [23].

We used intravenous LM infection [24] and a semi-quantitative immunofluorescence approach to investigate the capture and clearance of bacteria in the spleen. Previous histological studies showed that LM was trapped in the MZ of the spleen [25–27]. Clodronate-liposome depletion of MZ macrophages *in vivo* indicated that they were required for initial LM capture and control, but were dispensable for specific T-cell-mediated immunity [25]. At 24h following infection, LM was found primarily within CD11b^{+} and, to a less extent, CD11c^{+} cells [27]. More recently, CD8α^{+} DC were found to be the primary cell type containing viable bacteria early after infection (1–3 h) [28]. Other studies have detected LM exclusively in SIGN-R1^{+} MZM and not CD11c^{+} DC very early after infection [14]. Here, we identified five phagocyte populations that contained the bulk of LM after i.v. challenge. During the time when LM was in the MZ, its colocalization with MZM decreased dramatically. This shift in the cellular niche of LM *in vivo* has important implications for bacterial pathogenesis and protective host responses in the spleen.

Results

LM enters a wide variety of phagocytes immediately after challenge

We found that the recovery of LM (EGD)-infected host cells from spleen was unreliable; ~90% of LM CFU were lost in the process of isolating phagocytes and making single cell suspensions (Supporting Information Fig. 1). As an alternative, we developed an antibody staining approach, by which we identified five distinct phagocyte populations in spleen cryosections (Fig. 1 and Supporting Information Fig. 2). We observed three distinct macrophage subsets in their expected locations: F4/80[+] in the RP, MARCO[+] MZM in the outer MZ, and MOMA-1^{+} MMM in the inner MZ (Fig. 1A–C) [5, 9, 22, 29]. Nearly all ER-TR9^{+} MZM co-stained with antibodies to MARCO, suggesting that SIGN-R1^{+} cells are actually a subset of MARCO^{+} MZM (Fig. 1D). The CD11b^{hi} cells in our images appeared to be neutrophils, since they were smaller and rounder than macrophages and localized outside the white pulp (Fig. 1B, C, and F). Moreover, >95% of CD11b^{+} cells were Gr-1^{+} (Ly6G) and F4/80^{−} in co-stained sections (Fig. 1E and F). However, Gr-1 also reacts with the epitope Ly6C expressed on a number of other cell types, including inflammatory macrophages, making it difficult to define the CD11b^{+} population unambiguously. We found CD11c^{+} cells
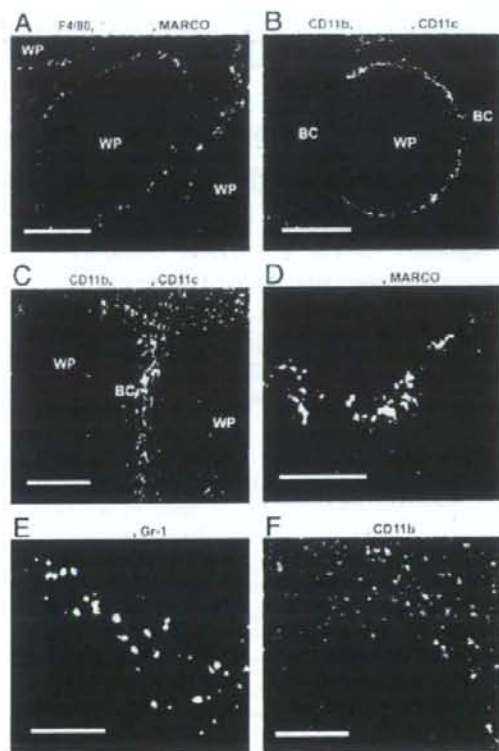
Figure 1. Histological characterization of resident phagocytes in the spleen. Cryosections from normal BALB/c mice were stained with different combinations of host cell markers to demonstrate staining specificity. (A) Anti-F4/80 (blue), anti-MOMA-1 (green), and anti-MARCO (red). (B) Anti-CD11b (blue), MOMA-1 (green), and CD11c (red). (C) Anti-CD11b (blue), anti-F4/80 (green), and anti-CD11c (red). (D) Anti-ER-TR9 (green) and anti-MARCO (red). Nearly all ER-TR9^{+} cells also express MARCO (yellow), suggesting that they are a subset of the MARCO^{+} MZM. (E) Anti-Gr-1 (green) and anti-CD11b (red). Approximately, 95% of CD11b^{+} cells are small, round and co-stained with Gr-1. (F) CD11b^{+} cells do not stain with F4/80, anti-F4/80 (green) and anti-CD11b (red). Scale bar = 200 μm in (A–C) and 100 μm in (D–F). Images are representative of three independent experiments. WP: white pulp. BC: bridging channel.

localized to the periarteriolar lymphoid sheath (PALS), the bridging channel and distributed sparsely in the RP and the MZ (Fig. 1B and C), also consistent with previous reports [30–32].

To reveal the host cells that interacted with LM immediately after infection, mice were injected with LM and sacrificed from minutes to hours later. Cryosections were prepared, stained with antibodies to LM and various host cell markers and the percentage of LM fluorescence signal overlap with each phagocyte surface marker (*i.e.* colocalization coefficient) was determined as described previously [33] (Fig. 2).

In contrast to previous reports [14, 28], LM entered a wide range of host phagocytes in the spleen (Fig. 2A). The percentage

of LM signal colocalized with each host cell type was as follows: F4/80$^+$ macrophages (26%), MARCO$^+$ macrophages (30%), MOMA-1$^+$ macrophages (19%), CD11b$^+$ cells (18%), and CD11c$^+$ DC (18%) and B220$^+$ cells (10%) (Fig. 2B). We included B220 staining as an internal negative control, because lymphocytes including B cells are not directly infected by LM. LM colocalization with B220 ranged from 5 to 10% in individual experiments. However, the covariance of LM and B220 signal was consistently negative (Pearson's correlation coefficient = −0.25), indicating that colocalization was less than that expected by chance alone, thus making B220 a suitable negative control. (The B220 stain may include plasmacytoid DC (pDC), but their contribution should be negligible since they represent less than 1% of spleen cells while B cells represent close to 50%.)

Histological analyses were performed at different concentrations of LM including those over the LD$_{50}$ dose (Fig. 2C). At the 10^6 dose, most phagocytes contained a single bacterium (Fig. 2A). At a higher dose (10^8), increased variation was observed with many cells containing one LM and others containing small clusters of LM (Fig. 2C). Despite a 100-fold increase in dose (from 10^6 to 10^8), the cellular distribution of LM remained remarkably similar at 30 min after injection (compare panel 2D with 2B in Fig. 2), with the exception that more LM was found in CD11b$^+$ cells with the larger inocula (38% up from 18%). We also gave mice a 20-fold lower dose of LM (5 × 10^4) and examined its distribution. Although the number of bacteria in each section was small and highly variable, we found numerous examples of LM colocalized to each of the five phagocyte populations (Supporting Information Fig. 3A and B), similar to experiments using 10^6 LM.

We also examined the colocalization of bacteria in a sublethal infection using attenuated LM strain MORO-2 (LD$_{50}$ ~3 × 10^6) [34], which behaves normally during the first few hours of infection, but can replicate only approximately three times in the host cytosoplasm due to a deficiency in lipoic acid utilization. The cellular distribution of 10^6 MORO-2 was indistinguishable from experiments using 10^6 EGD (Supporting Information Fig. 3C and D).

Next, we compared LM uptake with other known substrates of phagocytosis: fluorescent polystyrene beads and FITC-conjugated dextrans. At 30 min after injection, fluorescent beads were taken up by MZM and, to a much lesser extent, by CD11c$^+$ DC (Fig. 2E). The majority of beads (~76%) were associated with MARCO$^+$ cells, ~40% with MOMA-1$^+$ MMM, and <20% with CD11c$^+$ DC. Few, if any, beads were associated with CD11b$^+$ and F4/80$^+$ cells. FITC-conjugated dextran, which has been shown to be taken up specifically by MZM (MARCO$^+$ ER-TR9$^+$) via SIGN-R1 [7], was captured efficiently by MARCO$^+$ cells and accumulated to high levels by 30 min (Fig. 2F). The other phagocyte populations examined showed only background levels of colocalization with dextran (Fig. 2F), validating our analysis. Thus, the trapping of LM was unexpectedly promiscuous compared with the uptake of fluorescent beads and dextran.

It is important to note that the initial trapping compartment of LM was capable of controlling infection. We have infected wild-type 129/SvEv, as well as type I and type II interferon-deficient mice (IFNAR and IFNGR) and found limited to no growth of

bacteria between 30 min and 4 h post-infection in the spleen (Fig. 2G). This would suggest that the net ability of the MZ cells is to control LM independent of tonic interferon signaling.

The cellular niche of LM changes rapidly

The fate of LM in phagocytes was examined during the first hours of infection. From 30 min to 6 h, the amount of LM per cell in F4/80$^+$ and CD11c$^+$ cells held steady without an appreciable increase (Fig. 3A). For MOMA-1$^+$ cells, a slight increase at 2 h was observed; however, there was no significant difference between 30 min and 6 h. In contrast, LM signal in MARCO$^+$ and CD11b$^+$ cells decreased significantly (Fig. 3A). To determine whether this result also held true for ER-TR9$^+$ MZM, we examined LM colocalization with ER-TR9 (bright yellow spots in Fig. 3B) and found it decreased significantly at 2 and 6 h (Fig. 3B and C). In addition, we observed a marked decrease in covariance between LM and ER-TR9 signals over the first 6 h after infection (Fig. 3D). The total LM pixel per image remained relatively stable over this time (Fig. 3E) and was well correlated to the actual CFU counts per spleen (Fig. 3F). Moreover, host cell signal remained constant, with the exception of CD11b, which increased roughly 50% between 30 min and 6 h (Fig. 3G). We believe that the increased in CD11b$^+$ signal most likely represents the infiltration of cells because the signal increases rapidly and we did not detect a gradual rise in signal intensity on a per cell basis between 0.5 and 6 h (data not shown). After 6 h, LM is also detected in the PALS, the site of rapid exponential growth of LM in the spleen [27, 35].

At 12 h, approximately 40% of the LM signal in the MZ was found in CD11c$^+$ cells (Fig. 4A), while about 20% was found in each of the F4/80$^+$, MOMA-1$^+$, and CD11b$^+$ populations, similar to the 30 min time point. In contrast, only 5% of the LM signal was found in MARCO$^+$ MZM (compared with 30% at 30 min). By 24 h, when LM infection was confined primarily to the PALS, the cellular distribution of LM changed further (Fig. 4B). The majority of infected cells at 24 h were CD11b$^+$ cells (54%) and LM was barely detectable in MARCO$^+$ MZM (~2% colocalization). The percentage of colocalization with CD11c$^+$ cells also fell sharply to 22%. Both, F4/80$^+$ macrophages and MOMA-1$^+$ cells continued to show evidence of LM infection with colocalization coefficients of 17 and 18%, respectively.

Discussion

Defining the cellular niche occupied by bacteria in the spleen is fundamental for understanding how bacterial pathogenesis proceeds in vivo and how the host mounts a protective immune response. Our analysis showed that LM was taken up initially by a broad range of phagocytic cells, including macrophages (MARCO$^+$, ERT-R9$^+$, and F4/80), granulocytes (CD11b$^+$, Gr-1$^+$ cells) and DC (CD11c$^+$), in general agreement with a previous histological study [26]. These results contrast sharply with the conclusions of others that LM was captured exclusively by CD8a$^+$ DC [28] or
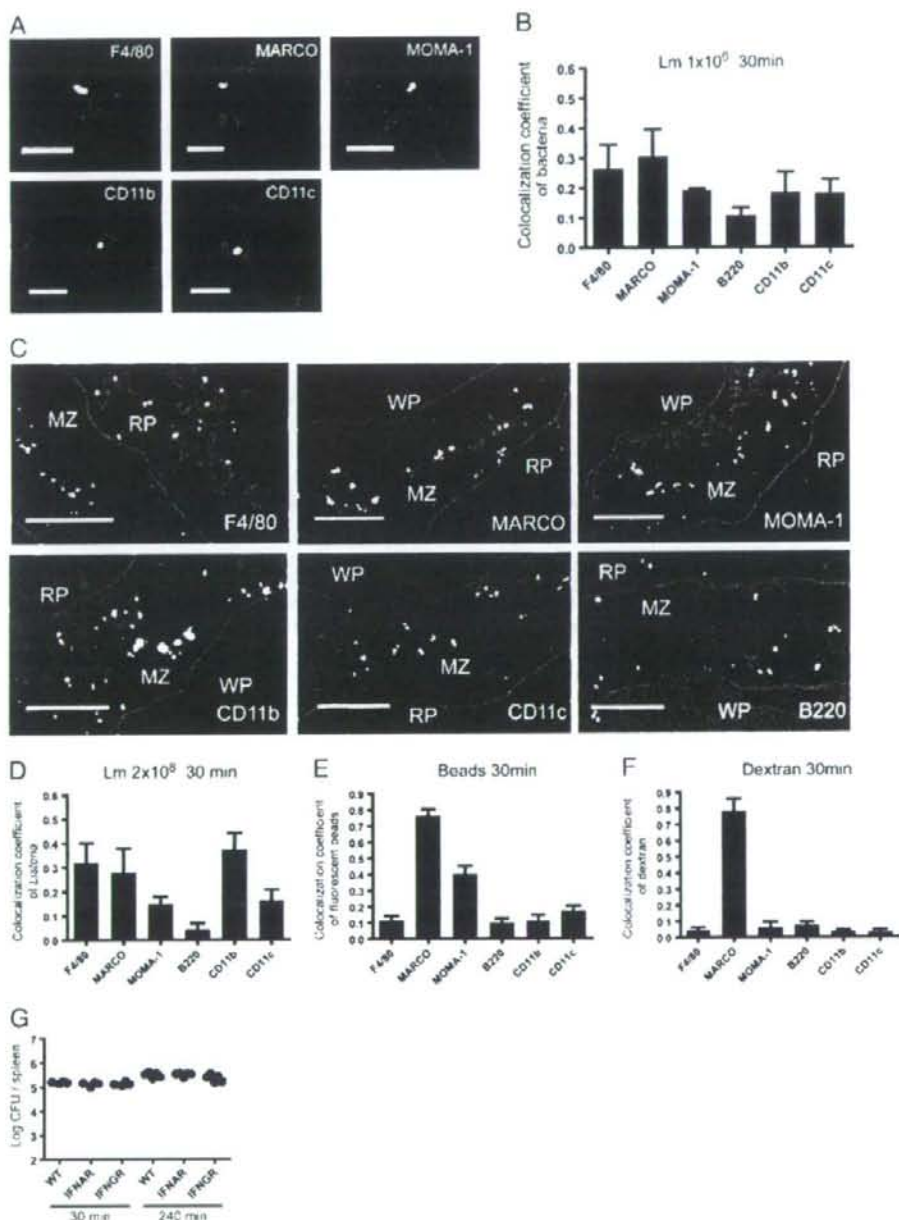
Figure 2. LM is broadly distributed in splenocytes immediately after i.v. infection. (A) Infected host cells in stained cryosections 30 min following infection with 10⁶ EGD strain of LM. LM (green) and host cell markers (red). Scale bar = 10 μm. Images are representative of three independent experiments. (B) LM colocalization with host cell types. Bars represent mean + SD of at least 30 images per each cell type. (C) Spleens at 30 min post infection with 2×10^8 LM. Cryosections were stained with phalloidin-Alexa Fluor 350, anti-LM (green) and indicated host-cells. Yellow represents colocalization between LM and stained host-cells. Blue lines represent the edge of the MZ determined by phalloidin staining. Scale bar = 50 μm. (D) Colocalization analysis of (D) 2×10^8 LM, (E) 7.2×10^8 fluorescent 1.0 μm beads, and (F) 200 μg of 70 kDa FITC-conjugated dextran with splenic phagocytes 30 min after i.v. injection. Bars represent mean + SD of ten images per cell type. (G) 129/SvEv, IFNAR, and IFNGR mice were infected intravenously with 10⁷ CFU of LM EGD strain and spleen colony counts were determined at 30 and 240 min post infection. MZ: marginal zone; RP: red pulp; WP: white pulp.
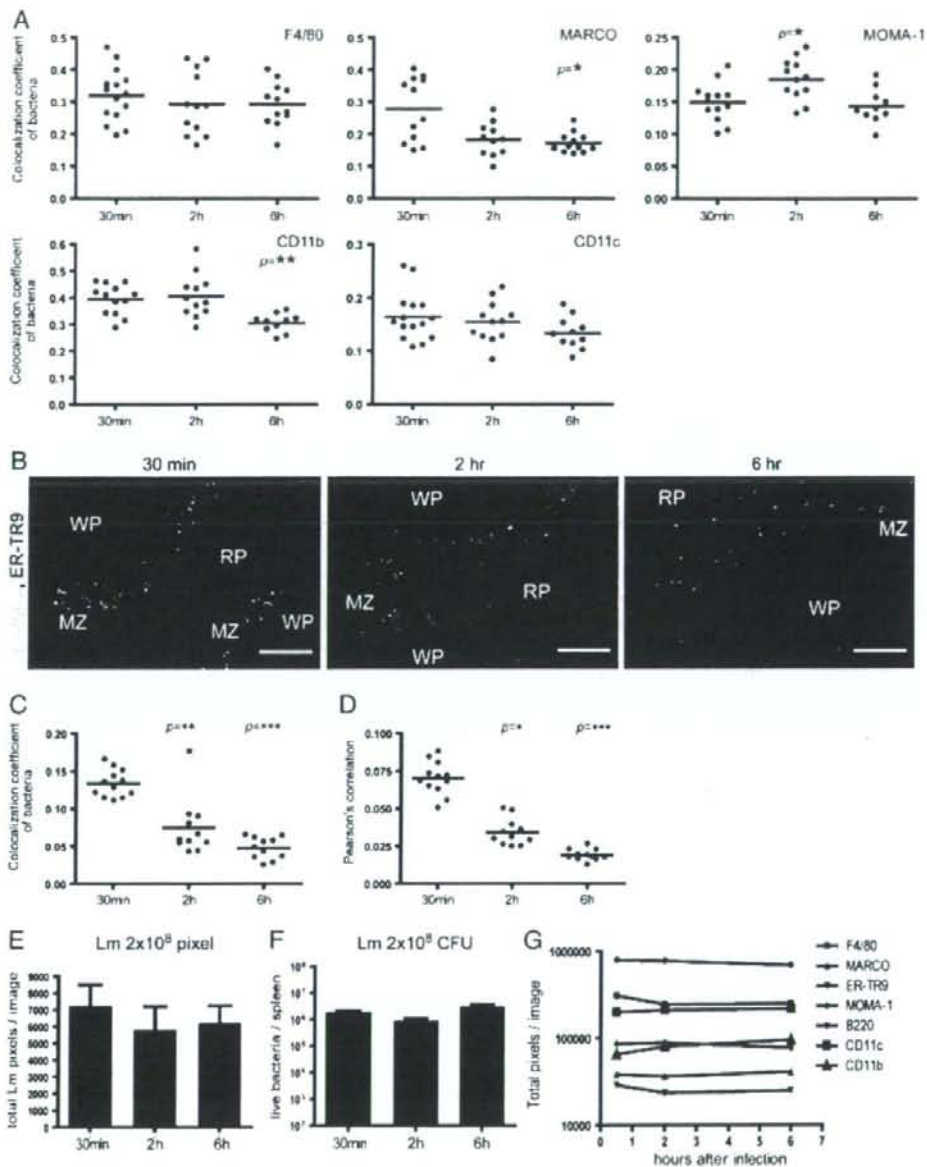
Figure 3. LM signal decreases in MZM 0.5–6 h post-infection. (A) The colocalization coefficients of LM and host cell markers over time. Scatter plots show mean values for individual images and pooled means. (B) Spleen sections from mice infected with 2×10^8 LM at 30 min, 2 h, and 6 h. Cryosections were stained with phallodin-Alexa Fluor 350, anti-LM (green) and anti-SIGNR1 (red). Colocalization between LM and host-cells appears yellow in the image. Blue lines highlight the MZ edge drawn based on phalloidin staining. Scale bar = 100 μm. Images are representative of ten images per time point. (C) Colocalization of LM in ER-TR9^{+} cells and (D) covariance of LM and ER-TR9 signal (Pearson's correlation), at increasing times after infection. Each dot is the mean value of a single image and pooled means are shown. (E) LM signal in pixels per image at 30 min, 2 h, and 6 h post infection (2×10^8 LM). Bars show mean+SD of 50 images per time point. (F) CFU per spleen 30 min, 2 h, and 6 h post infection (2×10^8 LM). Bars show mean+SD, five mice per group. (G) Host cell signal expressed in pixels per image at increasing times after infection. Graph shows mean of 12 images per group. All data are representative of three independent experiments with similar results. MZ: marginal zone; RP: red pulp; WP: white pulp.
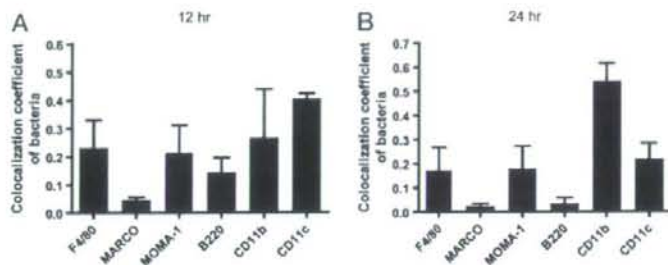
Figure 4. Host cell distribution of LM 12 and 24 h post infection. LM colocalization with splenic phagocytes 12 h (A) and 24 h (B) after infection. Bars represent mean+SD of ten images per cell type. Bar graphs are representative of three independent experiments. LM disappears rapidly from MARCO⁺ MZM, but increases transiently in CD11c⁺ cells.

ER-TR9⁺ macrophages [14]. Histological studies from independent groups concur that LM associates with resident macrophages in the MZ for several hours after infection, although the characterization of macrophages differed depending on the markers used to detect them [14, 25–27]. Neuenhahn et al. [28] detected only viable LM present in splenocytes isolated by cell sorting, but because MZM are difficult to recover from spleen tissue, these cells could be easily missed during data analysis.

We used a panel of five different antibodies to provide a comprehensive histological view of early LM infection in the spleen. The criteria for including antibodies in our analysis were (i) staining must be highly reproducible and the results entirely consistent with classical histological studies with regard to the morphology and anatomical location of splenic DC, MZM, metallophilic macrophages, granulocytes, and lymphocytes [4, 9, 31, 32, 36, 37], (ii) antibodies must stain distinct splenocyte populations with minimal overlap (verified by co-staining), and (iii) the percent colocalization with LM and each host cell marker must be reproducible and the colocalized LM signal must add up to ~100% of the total LM signal in our sections (i.e. to ensure that no major splenocyte populations are missed). Our analysis focused on the early stages of LM infection but it will be important to examine other splenocyte populations such as inflammatory monocytes, pDC, and tumor necrosis factor alpha and inducible nitric oxide synthase producing DC (Tip DC) [38, 39] at later times.

In addition, we assessed the robustness of our colocalization analysis with several control experiments. We found dextran colocalized strongly with MZM (MARCO⁺), but not other phagocytes, consistent with the fact that MZM express the dextran receptor SIGN-R1 [5]. Fluorescent beads were taken up by MARCO⁺ and MOMA-1⁺ macrophages, to a much lesser extent by CD11c⁺ cells and were undetectable in CD11b⁺ cells. The initial cellular niche of LM was strikingly promiscuous and our data suggest that LM might enter host cells via multiple receptors and phagocytic pathways.

During the first 4–6 h, when bacteria are located primarily in the MZ, LM growth appeared to be controlled. It was not only until LM was transported to the PALS that the exponential phase of LM growth took place. During this period the host cell distribution changed: the number of LM in MARCO⁺ (and ER-TR9⁺) macro-

phages decreased during the first few hours of infection, while it persisted in other cell types, such as CD11c⁺ DC and MOMA-1⁺ MMM. Whether the apparent control reflects a cytocidal activity of the MZM or is a reflection of cellular dynamics and turnover is not clear at this time. However, the capture of LM by MZM is undoubtedly important since clodronate-liposome depletion of these phagocytes augmented infection. Experiments are in progress to elucidate the mechanisms of LM control in the MZ, but our initial studies (Fig. 2G) indicate that this control is independent of either interferon-gamma or type-1 interferons. To note is that MARCO- and SIGN-R1-deficient mice were highly susceptible to pneumococcal infection [8, 40]. It will be interesting to compare and contrast LM infection with other bacteria such as Staphylococcus and Salmonella to determine whether the MZ control extends across bacterial species and possibly to viruses, as seen in LCMV infection [41, 42]. It is noteworthy that although RP macrophages do not appear to be listericidal, they apparently fail to support the proliferation of LM, since we did not detect an increase in the amount of LM in the F4/80⁺ cells during the time-frame of our experiments.

In contrast to the MZ stage of infection, LM signal increased explosively in the PALS from 12-24 h. The preferential replication of LM in the PALS might reflect decreased bactericidal capacity or alternatively PALS resident cells, such as DC, might be more permissive for LM proliferation. In fact, we observed a significant increase of LM in DC over the first 12 h of infection. Moreover the heightened and very extensive lymphocyte apoptosis in PALS has been shown to be in great part responsible for such strong expansion of LM [43].

Materials and methods

Mice

BALB/cJ mice were obtained from the Jackson Laboratory (Bar Harbor, ME) and were maintained and bred under specific pathogen free conditions in the Washington University mouse facility, in accordance with the guidelines of the Washington

University Committee for the Humane Care of Laboratory Animals and with National Institutes of Health guidelines on laboratory animal welfare.

Bacteria and fluorescent reagents

LM strain EGD was stored as frozen glycerol stocks ($\sim 1 \times 10^9$/mL) at $-80°C$. LM numbers in the spleen were estimated by determining CFU from tissue homogenates using standard procedures. For early time point experiments (30 min–6 h), bacteria were cultured in BHI medium and harvested during log phase growth for inoculation. LM concentrations in liquid cultures were estimated by optical density measurements using standard growth curves. For 12 and 24 time points, frozen stocks were thawed and diluted appropriately prior to i.v. injection. Our frozen stocks contained negligible dead bacteria (96.88% viability, $p = 0.48$) compared with starting cultures for up to 5 months. FluoSpheres carboxylate-modified microspheres (yellow green, $1.0 \mu m$) and Fluorescein-conjugated dextran (lysine-fixable, 70 kDa) were purchased from Invitrogen (Carlsbad, CA).

Histology

Spleens were harvested, embedded in OCT compound and $5 \mu m$ cryosections were prepared. Sections were fixed with 4% paraformaldehyde in PBS (pH 7.2) at $4°C$ for 5 min and blocked with StartingBlock Blocking Buffer (Thermo Fisher Scientific, Rockford, IL) for 10 min, then sequentially incubated with purified and/or biotin-conjugated primary antibodies and fluorescent-dye-conjugated secondary antibodies and/or fluorescent-dye-conjugated streptavidin. Antibodies and reagents used for staining were as follows: phalloidin-Alexa Fluor 350 (Invitrogen), rat anti-mouse F4/80 (biotin conjugated, BM8; eBioscience, San Diego, CA).

Rat anti-mouse/human CD45R/B220 (PE or Alexa Fluor 647 conjugated, RA3-6B2; eBioscience, or BD Biosciences, San Jose, CA), rat anti-mouse MARCO (PE-conjugated, ED31; Serotec, Oxford, UK), rat anti-mouse SIGN-R1 (biotin-conjugated, ER-TR9; BMA Biomedicals, Augst, Switzerland).

Rat anti-mouse siglec-1 (biotin or FITC-conjugated, MOMA-1; BMA Biomedicals or Serotec), hamster anti-mouse CD11c (biotin or PE-conjugated, HL3 or N418; BD Biosciences or eBioscience), rat anti-mouse CD11b (biotin, Alexa Fluor 647 or PE-conjugated, M1/70; BD Biosciences or eBioscience), rabbit anti-LM polyserum serotypes 1 and 4 (BD Diagnostic Systems, Sparks, MD), goat anti-rabbit IgG (FITC-conjugated; Sigma, St. Louis, MO), streptavidin (Alexa Fluor 555 or Alexa Fluor 647-conjugated; Invitrogen), rat anti-mouse Ly-6G(Gr-1) (PE-conjugated, RB6-8C5; eBioscience).

Immunofluorescence microscopy

Four-color fluorescence microscopy of cryosections was performed using an Olympus BX51 equipped with 100 W mercury lamp (Olympus America, Center Valley, PA) and a SPOT RT charge-coupled device camera (Diagnostic Instruments, Sterling Heights, MI). Monochrome images ($1200 \, pi \times 1600 \, pi = 885 \times 1180 \mu m$ in $10 \times$ objectives; $440 \times 586 \mu m$ in $20 \times$ objectives, 12-bit ;depth) were acquired with filter sets optimized for DAPI, FITC, tetramethyl rhodamine isothiocyanate (TRITC), and cyanine dye 5(y5, 670 nm emission), respectively (Chroma, Rockingham, VT). Exposure times of 1–2 s were used and a linear contrast stretch was applied to the images to normalize brightness. Monochrome images were pseudo-colored and merged into 24 bit RGB images with SPOT RT camera software and exported into Adobe Photoshop for subsequent color balancing and image segmentation. Colocalization coefficients and Pearson's correlation coefficients [33] were generated from pooled fluorescent images with Volocity software (version 3.7; Improvision, Waltham, MA). Color-balanced images were transferred to Volocity and RGB channels were split. Thresholds were set for each channel using automatic thresholding and were confirmed by eye; in cases where automatic thresholding failed, thresholds were re-adjusted manually comparable to other images. All data from three time points (30 min, 2 h, and 6 h) were first tested with One-way ANOVA (Kruskal–Wallis test, nonparametric). If the overall p-value was < 0.05, 30 min versus 2 h, and 30 min versus 6 h were secondarily tested with the Dunns test. $^*p<0.05$, $^{**}p<0.01$, $^{***}p<0.001$.

Conflict of interest: The authors declare no financial or commercial conflict of interest.

References

1 Junt, T., Scandella, E. and Ludewig, B., Form follows function: lymphoid tissue microarchitecture in antimicrobial immune defence. Nat. Rev. Immunol. 2008. 8: 764–775.

2 Khanna, K. M. and Lefrançois, L., Geography and plumbing control the T cell response to infection. Immunol. Cell Biol. 2008. 86: 416–422.

3 Kraal, G., Cells in the marginal zone of the spleen. Int. Rev. Cytol. 1992. 132: 31–74.

4 Mebius, R. E. and Kraal, G., Structure and function of the spleen. Nat. Rev. Immunol. 2005. 5: 606–616.

5 Eloman, O., Kangas, M., Sahlberg, C., Tuukkanen, J., Sormunen, R., Liakka, A., Thesleff, I. et al., Cloning of a novel bacteria-binding receptor structurally related to scavenger receptors and expressed in a subset of macrophages. Cell 1995. 80: 603–609.

6 Sankala, M., Brannstrom, A., Schulthess, T., Bergmann, U., Morgunova, E., Engel, J., Tryggvason, K. and Pikkarainen, T., Characterization of recombinant soluble macrophage scavenger receptor MARCO. J. Biol. Chem. 2002. 277: 33378–33385.

7 Kang, Y. S., Yamazaki, S., Iyoda, T., Pack, M., Bruening, S.A., Kim, J. Y., Takahara, K. et al., SIGN-R1, a novel C-type lectin expressed by marginal zone macrophages in spleen, mediates uptake of the polysaccharide dextran. Int. Immunol. 2003. 15: 177–186.

8 Lanoue, A., Clatworthy, M. R., Smith, P., Green, S., Townsend, M. J., Jolin, H. E., Smith, K. G. et al., SIGN-R1 contributes to protection against lethal pneumococcal infection in mice. J. Exp. Med. 2004. 200: 1383–1393.

9 Kraal, G. and Janse, M., Marginal metallophilic cells of the mouse spleen identified by a monoclonal antibody. Immunology 1986. 58: 665–669.

10 Jones, C., Virji, M. and Crocker, P. R., Recognition of sialylated meningococcal lipopolysaccharide by siglecs expressed on myeloid cells leads to enhanced bacterial uptake. Mol. Microbiol. 2003. 49: 1213–1225.

11 Oetke, C., Kraal, G. and Crocker, P. R., The antigen recognized by MOMA-1 is sialoadhesin. Immunol. Lett. 2006. 106: 96–98.

12 Crocker, P. R., Kelm, S., Dubois, C., Martin, B., McWilliam, A. S., Shotton, D. M., Paulson, J. C. and Gordon, S., Purification and properties of sialoadhesin, a sialic acid-binding receptor of murine tissue macrophages. EMBO J. 1991. 10: 1661–1669.

13 Eloranta, M. L. and Alm, G. V., Splenic marginal metallophilic macrophages and marginal zone macrophages are the major interferon-alpha/beta producers in mice upon intravenous challenge with herpes simplex virus. Scand. J. Immunol. 1999. 49: 391–394.

14 Jablonska, J., Dittmar, K. E., Kleinke, T., Buer, J. and Weiss, S., Essential role of CCL2 in clustering of splenic ERTR-9+macrophages during infection of BALB/c mice by Listeria monocytogenes. Infect. Immun. 2007. 75: 462–470.

15 Nathan, C., Neutrophils and immunity: challenges and opportunities. Nat. Rev. Immunol. 2006. 6: 173–182.

16 Conlan, J. W. and North, R. J., Neutrophils are essential for early anti-Listeria defense in the liver, but not in the spleen or peritoneal cavity, as revealed by a granulocyte-depleting monoclonal antibody. J. Exp. Med. 1994. 179: 259–268.

17 Czuprynski, C. J., Brown, J. F., Maroushek, N., Wagner, R. D. and Steinberg, H., Administration of anti-granulocyte mAb RB6-8C5 impairs the resistance of mice to Listeria monocytogenes infection. J. Immunol. 1994. 152: 1836–1846.

18 Rogers, H. W. and Unanue, E. R., Neutrophils are involved in acute, nonspecific resistance to Listeria monocytogenes in mice. Infect. Immun. 1993. 61: 5090–5096.

19 Unanue, E. R., Inter-relationship among macrophages, natural killer cells and neutrophils in early stages of Listeria resistance. Curr. Opin. Immunol. 1997. 9: 35–43.

20 Witmer, M. D. and Steinman, R. M., The anatomy of peripheral lymphoid organs with emphasis on accessory cells: light-microscopic immunocytochemical studies of mouse spleen, lymph node, and Peyer's patch. Am. J. Anat. 1984. 170: 465–481.

21 Dudziak, D., Kamphorst, A. O., Heidkamp, G. F., Buchholz, V. R., Trumpfheller, C., Yamazaki, S., Cheong, C. et al., Differential antigen processing by dendritic cell subsets in vivo. Science 2007. 315: 107–111.

22 Austyn, J. M. and Gordon, S., F4/80, a monoclonal antibody directed specifically against the mouse macrophage. Eur. J. Immunol. 1981. 11: 805–815.

23 Oldenborg, P. A., Zheleznyak, A., Fang, Y. F., Lagenaur, C. F., Gresham, H. D. and Lindberg, F. P., Role of CD47 as a marker of self on red blood cells. Science 2000. 288: 2051–2054.

24 Pamer, E. G., Immune responses to Listeria monocytogenes. Nat. Rev. Immunol. 2004. 4: 812–823.

25 Aichele, P., Zinke, J., Grode, L., Schwendener, R. A., Kaufmann, S. H. and Seiler, P., Macrophages of the splenic marginal zone are essential for trapping of blood-borne particulate antigen but dispensable for induction of specific T cell responses. J. Immunol. 2003. 171: 1148–1155.

26 Conlan, J. W., Early pathogenesis of Listeria monocytogenes infection in the mouse spleen. J. Med. Microbiol. 1996. 44: 295–302.

27 Muraille, E., Giannino, R., Guirnalda, P., Leiner, I., Jung, S., Pamer, E. G. and Lauvau, G., Distinct in vivo dendritic cell activation by live versus killed Listeria monocytogenes. Eur. J. Immunol. 2005. 35: 1463–1471.

28 Neuenhahn, M., Kerksiek, K. M., Nauerth, M., Suhre, M. H., Schiemann, M., Gebhardt, F. E., Stemberger, C. et al., CD8alpha+dendritic cells are required for efficient entry of Listeria monocytogenes into the spleen. Immunity 2006. 25: 619–630.

29 Dijkstra, C. D., Van Vliet, E., Dopp, E. A., van der Lelij, A. A. and Kraal, G., Marginal zone macrophages identified by a monoclonal antibody: characterization of immuno- and enzyme-histochemical properties and functional capacities. Immunology 1985. 55: 23–30.

30 Metlay, J. P., Witmer-Pack, M. D., Agger, R., Crowley, M. T., Lawless, D. and Steinman, R. M., The distinct leukocyte integrins of mouse spleen dendritic cells as identified with new hamster monoclonal antibodies. J. Exp. Med. 1990. 171: 1753–1771.

31 Mitchell, J., Lymphocyte circulation in the spleen. Marginal zone bridging channels and their possible role in cell traffic. Immunology 1973. 24: 93–107.

32 Steinman, R. M., Pack, M. and Inaba, K., Dendritic cells in the T-cell areas of lymphoid organs. Immunol. Rev. 1997. 156: 25–37.

33 Manders, E. M. M., Verbeek, F. J. and Aten, J. A., Measurement of colocalization of objects in dual-color confocal images. J. Microsc.-Oxford 1993. 169: 375–382.

34 O'Riordan, M., Moors, M. A. and Portnoy, D. A., Listeria intracellular growth and virulence require host-derived lipoic acid. Science 2003. 302: 462–464.

35 Aoshi, T., Zinselmeyer, B. H., Konjufca, V., Lynch, J. N., Zhang, X., Koide, Y. and Miller, M. J., Bacterial entry to the splenic white pulp initiates antigen presentation to CD8+T cells. Immunity 2008. 29: 476–486.

36 Taylor, P. R., Martinez-Pomares, L., Stacey, M., Lin, H. H., Brown, G. D. and Gordon, S., Macrophage receptors and immune recognition. Annu. Rev. Immunol. 2005. 23: 901–944.

37 Nussenzweig, M. C., Steinman, R. M., Witmer, M. D. and Gutchinov, B., A monoclonal antibody specific for mouse dendritic cells. Proc. Natl. Acad. Sci. USA 1982. 79: 161–165.

38 Serbina, N. V., Salazar-Mather, T. P., Biron, C. A., Kuziel, W. A. and Pamer, E. G., TNF/iNOS-producing dendritic cells mediate innate immune defense against bacterial infection. Immunity 2003. 19: 59–70.

39 Tam, M. A. and Wick, M. J., Differential expansion, activation and effector functions of conventional and plasmacytoid dendritic cells in mouse tissues transiently infected with Listeria monocytogenes. Cell. Microbiol. 2006. 8: 1172–1187.

40 Arredouani, M., Yang, Z., Ning, Y., Qin, G., Soininen, R., Tryggvason, K. and Kobzik, L., The scavenger receptor MARCO is required for lung defense against pneumococcal pneumonia and inhaled particles. J. Exp. Med. 2004. 200: 267–272.

41 Odermatt, B., Eppler, M., Leist, T. P., Hengartner, H. and Zinkernagel, R. M., Virus-triggered acquired immunodeficiency by cytotoxic T-cell-dependent destruction of antigen-presenting cells and lymph follicle structure. *Proc. Natl. Acad. Sci. USA* 1991. 88: 8252–8256.

42 Seiler, P., Aichele, P., Odermatt, B., Hengartner, H., Zinkernagel, R. M. and Schwendener, R. A., Crucial role of marginal zone macrophages and marginal zone metallophils in the clearance of lymphocytic choriomeningitis virus infection. *Eur. J. Immunol.* 1997. 27: 2626–2633.

43 Carrero, J. A., Calderon, B. and Unanue, E. R., Lymphocytes are detrimental during the early innate immune response against *Listeria monocytogenes. J. Exp. Med.* 2006. 203: 933–940.

Abbreviations: **LM:** *Listeria monocytogenes* · **MARCO:** macrophage receptor with collagenous structure · **MMM:** metallophilic marginal zone macrophage · **MZ:** marginal zone · **MZM:** marginal zone macrophage · **PALS:** periarteriolar lymphoid sheath · **pDC:** plasmacytoid DC · **RP:** red pulp

Full correspondence: Dr. Mark J. Miller, Department of Pathology and Immunology, Washington University School of Medicine, St. Louis, MO 63110, USA
Fax: +1-314-362-4096
e-mail: miller@pathology.wustl.edu

Additional correspondence: Dr. Emil R. Unanue, Department of Pathology and Immunology, Washington University School of Medicine, St. Louis, MO 63110, USA.
e-mail: unanue@wustl.edu

Bacterial Entry to the Splenic White Pulp Initiates Antigen Presentation to CD8+ T Cells

Taiki Aoshi,[1] Bernd H. Zinselmeyer,[1,3] Vjollca Konjufca,[1,3] Jennifer N. Lynch,[1] Xin Zhang,[1] Yukio Koide,[2] and Mark J. Miller[1,*]

[1]Department of Pathology and Immunology, Washington University School of Medicine, 660 South Euclid Avenue, St. Louis, MO 63110, USA
[2]Department of Infectious Diseases, Hamamatsu University School of Medicine, 1-20-1 Handayama, Higashi-ku, Hamamatsu, Shizuoka 431-3192, Japan
[3]These authors contributed equally to this work
*Correspondence: miller@pathology.wustl.edu
DOI 10.1016/j.immuni.2008.06.013

SUMMARY

The spleen plays an important role in host-protective responses to bacteria. However, the cellular dynamics that lead to pathogen-specific immunity remain poorly understood. Here we examined *Listeria monocytogenes* (Lm) infection in the mouse spleen via in situ fluorescence microscopy. We found that the redistribution of Lm from the marginal zone (MZ) to the periarteriolar lymphoid sheath (PALS) was inhibited by pertussis toxin and required the presence of CD11c+ cells. As early as 9 hr after infection, we detected infected dendritic cells in the peripheral regions of the PALS and clustering of Lm-specific T cells by two-photon microscopy. Pertussis toxin inhibited both Lm entry into the PALS and antigen presentation to CD8+ T cells. Our study suggests that splenic dendritic cells rapidly deliver intracellular bacteria to the T cell areas of the white pulp to initiate CD8+ T cell responses.

INTRODUCTION

The spleen is a highly structured lymphoid organ consisting of three main compartments: the red pulp (RP) where red blood cells are captured and recycled, the marginal zone (MZ) containing marginal zone B cells and phagocytes positioned along the marginal sinus, and the white pulp (WP) where the majority of T cells and B cells reside (Mebius and Kraal, 2005). As microbes enter the marginal sinus of the spleen, they come in contact with a variety of splenic phagocytes, including macrophages, dendritic cells (DCs), and granulocytes (Kraal, 1992). DCs play an important role in carrying antigen from peripheral tissues to draining lymph nodes to trigger the adaptive immune response (Angeli and Randolph, 2006); however, an analogous picture for how antigen transport and presentation takes place in the spleen is lacking. Experiments that use low-dose clodronate-liposome treatment to selectively deplete marginal zone macrophages (MZM) showed that these cells were not required for adaptive immunity to *Listeria monocytogenes* (Lm) (Aichele et al., 2003). An important role for DCs in immunity to Lm infection was more formally demonstrated via the CD11c-DTR

system to deplete DCs (Jung et al., 2002; Muraille et al., 2005; Neuenhahn et al., 2006). The issue of whether bacterial antigen transport to the periarteriolar lymphoid sheath (PALS) of the spleen is required for antigen presentation to T cells has been raised by others (Muraille et al., 2005; Kursar et al., 2005) but has not been investigated directly.

To investigate how antigen presentation occurs in the spleen, we used the Lm infection model. Lm is a Gram-positive intracellular bacterium widely used to study innate and adaptive immunity in mice (Mackaness, 1962; Pamer, 2004; Unanue, 1997). After intravenous (i.v.) injection, Lm infects the liver and spleen, proliferates in these tissues for several days, and is eventually cleared by Lm-specific T cell responses. Mice that survive Lm challenge develop long-lasting CD8+ T cell immunity (Busch et al., 1998; Lauvau et al., 2001; Shedlock and Shen, 2003; Sun and Bevan, 2003). Although T cell responses to Lm infection have been studied extensively, only recently has the impact of tissue structure on Lm pathogenesis and development of host responses been examined in situ (Khanna et al., 2007).

Here, we provide evidence that DCs in the spleen transport bacteria from the MZ to the PALS for antigen presentation to T cells, analogous to their role in carrying antigens from peripheral tissues to draining lymph nodes. As early as 9 hr after infection, we observed the clustering of Lm-specific T cells in the PALS by two-photon (2P) microscopy, indicating that antigen recognition occurs rapidly in the spleen. Preventing the entry of Lm into the PALS by pretreating mice with pertussis toxin (PTx) inhibited both the progression of Lm infection and the initiation of antigen presentation to CD8+ T cells.

RESULTS

PTx Treatment Inhibits Lm Entry into PALS

We quantitatively examined the tissue distribution of bacteria during splenic infection. Lm was injected i.v. into BALB/c mice, and at different times after infection, spleen cryosections were stained with antibodies to Lm and B220 and with phalloidin (Muraille et al., 2005) to identify the major spleen compartments (Figure S1 available online). Lm redistributed dramatically from MZ and RP to the PALS over the first 24 hr of infection (Figures 1A and 1B), consistent with previous histological studies (Conlan, 1996; Muraille et al., 2005). Initially, bacteria were found primarily in the MZ (~65%) and RP (~30%) (2 hr, Figures 1A and 1C). Lm was not observed in the PALS before 6 hr but was
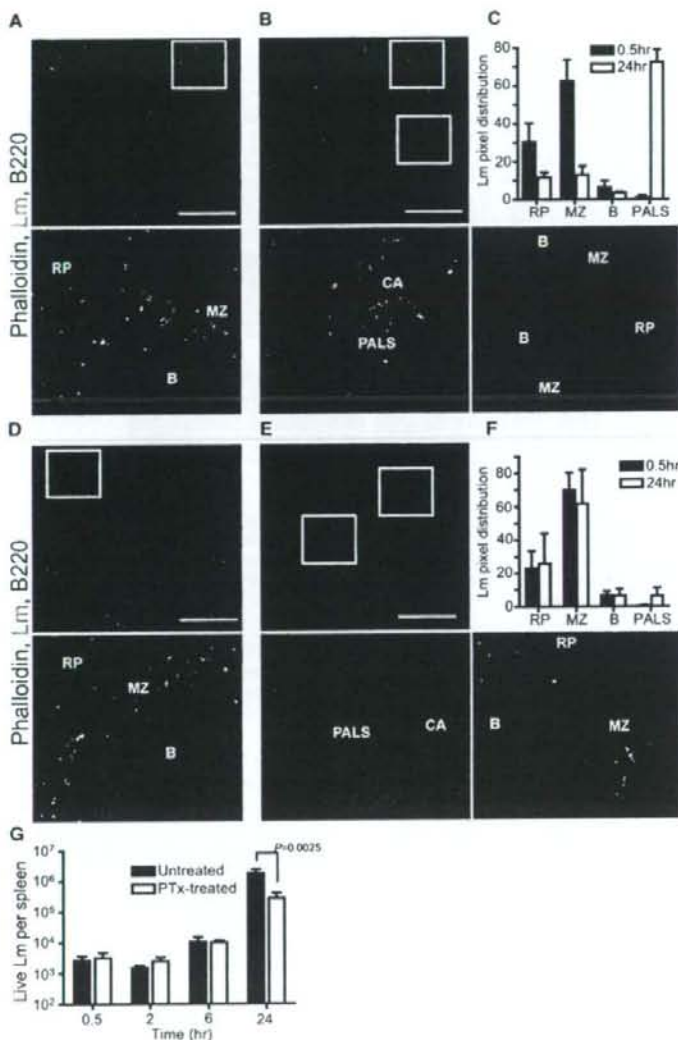
Figure 1. PTx Prevents Lm Translocation to the PALS and Decreases CFUs in the Spleen

(A) Spleen sections of mice 0.5 hr after infection with 10^7 Lm. Cryosections were stained with phalloidin-Alexa350 (blue), Lm antibody (green), and anti-B220-PE (red). Lower panels show magnified regions (white squares in upper panels). Scale bar represents 50 μm.

(B) Spleen sections of mice 24 hr after infection with 10^5 Lm. At 24 hr, many Lm are observed in the PALS area and few in the MZ and RP. Scale bar represents 50 μm.

(C) Quantification of Lm distribution in the spleen at 0.5 hr (black bar) and 24 hr (white bar) after infection (10 pooled nonoverlapping images from 2 mice). The splenic compartments: RP, red pulp; MZ, marginal zone; B, B cell follicle; and PALS, T cell area were separated as described in Figure S1.

(D and E) Spleen sections of PTx pretreated mice at 0.5 hr (D) and 24 hr (E) after infection. Scale bars represent 50 μm. Lower panels show magnified regions (white squares in upper panels).

(F) Lm distribution in the spleen of PTx-pretreated mice at 0.5 hr (black bar) and 24 hr (white bar) after infection (10 pooled nonoverlapping images from 2 mice).
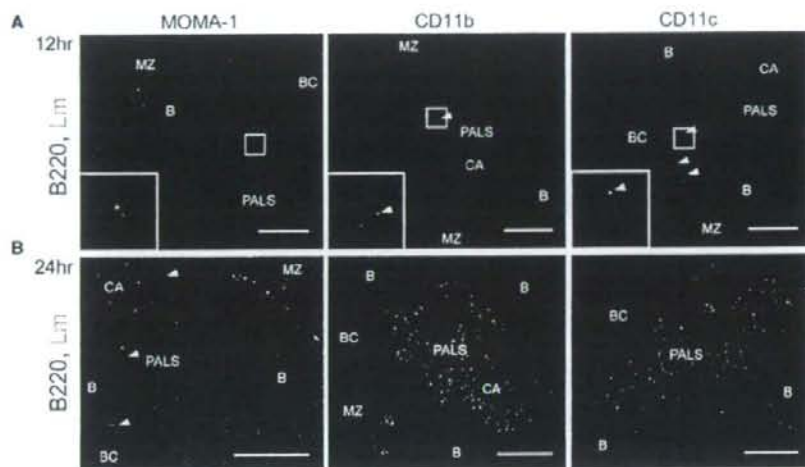
(G) CFU per spleen in PTx-untreated mice (black bar) and PTx-pretreated mice (white bar) at 0.5 hr to 24 hr after infection with Lm (two separate experiments, n = 5 to 7 mice per group). The p value (0.0025) was calculated with a two-tailed Mann-Whitney U-test.

dose) and analyzed their distribution in the absence of infection. Beads were found exclusively in the MZ and RP at 2 hr and only a few entered the PALS at 24 hr (Figures S2A and S2B). Next we coinjected high molecular weight dextran and Lm to determine whether infection alters access to the WP (Figure S2C). Dextran remained outside the PALS 2 hr after coinjection with Lm, indicating that infection did not markedly affect conduit permeability over this time. We also injected 0.5 μm beads (approximately the diameter of Lm) 4 hr after infection and found that the beads localized to the MZ and RP and did not enter the PALS. Moreover, live Lm in the spleen is insensitive to the cell-impermeable antibiotic gentamicin within minutes of i.v. challenge (Figure S2D), suggesting that bacteria are intracellular and not free to enter the PALS independently.

We postulated that Lm entry into the PALS requires the migration of host cells. To test this hypothesis, we treated mice with 500 ng pertussis toxin (PTx) i.p. and then examined Lm tissue distribution at 0.5 and 24 hr after Lm challenge (Figures 1D and 1F). PTx has been shown to block G protein-mediated (Gαi) chemokine receptor signaling and to inhibit leukocyte trafficking (Ato et al., 2004; Huang et al., 2007; Itano et al., 2003; Okada and Cyster, 2007). PTx treatment did not change the initial tissue

detected in low numbers at 9 hr and 12 hr (data not shown). After 24 hr, the distribution of Lm was reversed and the vast majority of bacteria were located in the PALS of the WP (~70%), with some bacteria (~20%) remaining in the MZ and RP (Figures 1B and 1C).

Soluble substances (~75 kD) can flow directly from the MZ into the white pulp through a conduit network (Mebius and Kraal, 2005). Although bacteria are presumably too large to access the PALS via this conduit network, we examined the possibility that Lm might alter conduit permeability and flow directly into the WP to initiate PALS infection. First, we injected a large number of 1 μm fluorescent beads (~10^8 or 1000 times more than the Lm

Figure 2. Lm-Infected Host Cells in the PALS

Immunofluorescence images of Lm and various host cell markers in spleen at 12 hr (A) and 24 hr (B) after infection. Cryosections were stained for B220 (blue), Lm (green), and the antibodies to host cell markers as indicated in the figure. Scale bars represent 100 μm. Lm was associated with CD11b⁺ and CD11c⁺ cells at 12 hr in the PALS (white arrows) but not with MOMA-1⁺ metallophilic marginal zone macrophages. At 24 hr after infection, bacteria shown as yellow spots in the image associated with CD11b⁺ cells and CD11c cells. Lm in MOMA-1⁺ cells is indicated with white arrows. The lower left inset shows a magnified region in the white square. Images are representative of at least three independent experiments.

distribution or the amount of Lm detected in spleen sections (Figures 1D and 1F); however, it profoundly inhibited Lm entry into the PALS (~99% decrease) 24 hr after challenge (Figures 1E and 1F). The early trapping and growth of Lm appeared normal after PTx treatment because Lm colony-forming units (CFU) in PTx-treated and control mice were similar for up to 6 hr (Figure 1G), and the initial cellular distribution of Lm appeared unaffected by PTx (data not shown). At 24 hr after infection, when Lm proliferation takes place primarily in the PALS, the number of viable bacteria was markedly reduced (~90% decreased) compared with untreated mice (Figure 1G). Thus, the reduced number of bacteria in the PALS after PTx treatment is primarily due to inhibition of bacterial entry and not due to effects on Lm capture or growth during the early stage of infection.

Spleen Remodeling in Response to Lm Infection

We examined the distribution of host cells in the spleen before and after infection to identify the cell types that migrate to the PALS and possibly transport Lm. In uninfected mice, host cell populations were observed in their expected locations in the spleen (Figure S3A). At 12 hr, Lm colocalized with CD11b⁺ cells in the PALS and CD11c⁺ cells primarily near the bridging channel, a structure that connects the WP to the RP (Figure 2A; Metlay et al., 1990; Mitchell, 1973). Metallophillic marginal zone macrophages (MOMA-1⁺) (Figure 2A; Kraal and Janse, 1986) had not entered the PALS in substantial numbers at this time. By 24 hr after infection, the number of MOMA-1⁺, CD11b⁺, and CD11c⁺ cells had increased in the PALS (Figure S3B). In contrast, F4/80⁺ (RP macrophages), MARCO⁺ (Elomaa et al., 1995), and ER-TR9⁺ (MZM) (Dijkstra et al., 1985) remained in their expected locations, similar to uninfected controls (Figures

S3A and S3B). At 24 hr, we found extensive Lm growth in the PALS and many CD11b⁺ cells contained Lm at foci of infection (Figure 2B). Bacteria were also found in MOMA-1⁺ (Figure 2B, arrowhead) and CD11c⁺ cells, although in lower numbers than observed for CD11b⁺ cells.

Lm Entry into PALS Requires CD11c⁺ Cells

To determine which cells are involved in Lm invasion of the PALS, we took advantage of the different recovery kinetics of splenic macrophages and DCs after clodronate-liposome-mediated depletion (van Rooijen et al., 1989) and looked for an association between host-cell recovery and Lm infection of the PALS.

The injection of clodronate liposomes ablated splenic macrophages by day 2 after treatment and these cells remained depleted for at least 1 week (Figure S4), as reported previously (van Rooijen et al., 1989). In our hands, clodronate liposomes also depleted CD11c⁺ cells by day 2, but these cells recovered substantially by day 6 (Figure S4). Similar DC recovery kinetics were observed in work with the CD11c-DTR transgenic system (Jung et al., 2002) and is consistent with the high turn-over rate (3 days) reported for splenic CD11c⁺ cells (Kamath et al., 2000). Notably, CD11b⁺ cells were not depleted by clodronate liposome treatment and appeared to slightly increase in number by day 2 (Figure S4). The CD11b⁺ cells identified in our sections are most likely granulocytes (~95% are F4/80⁻ and Gr-1⁺, data not shown) and recently recruited inflammatory monocytes or tumor necrosis factor-alpha and inducible nitric oxide synthase-producing DCs (TipDCs) (Serbina et al., 2003).

To determine which cells play a role in the translocation of Lm to PALS, we depleted splenocytes with clodronate liposomes, then infected mice with Lm on either day 2 or 6 after clodronate
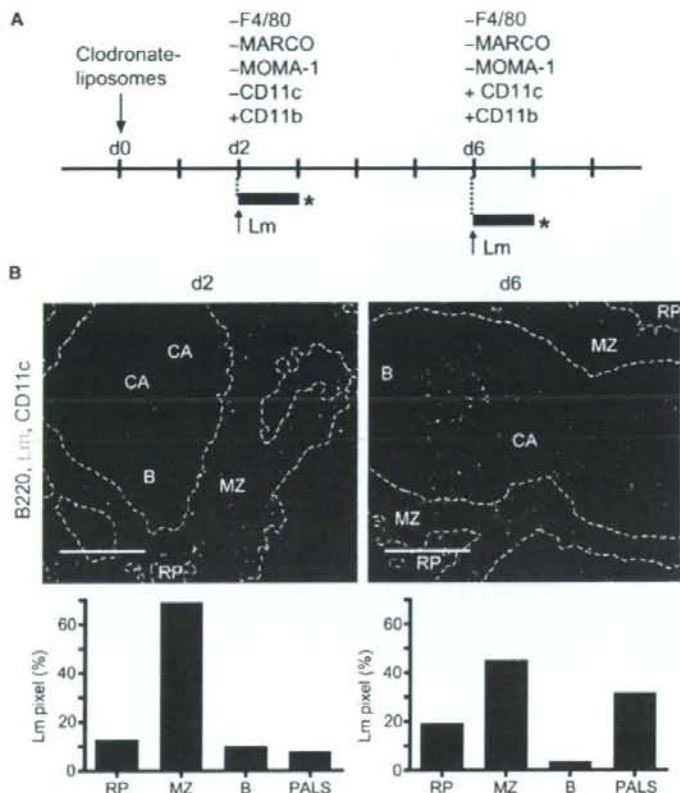
Figure 3. CD11c⁺ Recovery after Clodronate-Liposome Depletion Correlates with PALS Infection

(A) Outline of the experimental protocol. Clodronate liposomes were prepared as described previously and administered to deplete splenocytes 2 or 6 days prior to infection. Mice were infected with 10^6 Lm and sections were stained for CD11c (red) and Lm (green) to assess the degree of PALS infection 24 hr later (asterisk).

(B) Spleen cryosections from clodronate-treated mice (top) infected on day 2 (left) or day 6 (right). Scale bars represent 200 μm. Dashed lines indicate MZ regions based on phalloidin staining (blue). Quantitative analysis (bottom) of Lm distribution in splenic compartments. Data are representative of two or more independent experiments.

administration. The PALS was examined 24 hr later for the presence of Lm (Figure 3A). In mice infected on day 2, when both macrophages and CD11c cells were depleted, the vast majority of bacteria (~70%) were found in the MZ (Figure 3B, left) and <10% of the total Lm signal was present in the PALS, compared to ~70% in infected mock-depleted controls (Figure 1B). In mice infected on day 6 after clodronate treatment, when CD11c⁺ cells had recovered but macrophages had not, widespread Lm growth in the PALS was observed (Figure 3B, right), suggesting that DCs play an important role in the progression of Lm infection to the PALS. Because CD11b⁺ cells are present on day 2 when Lm remains in the MZ, these cells do not play a dominant role in the initial entry of Lm into the PALS, but most likely follow the bacteria into the PALS once it becomes infected. The close association between DC appearance and PALS infection was confirmed by means of CD11c-DTR mice (Jung et al., 2002) and a similar cell depletion and recovery approach (Figure S5).

The Arrival of Infected DCs in the PALS Initiates Antigen Presentation

The precise location of T cell priming in the spleen is unknown. T cells are most abundant in the PALS; however, they are also found in the RP and MZ and antigen presentation could occur in these compartments as well. Based on our depletion and recovery results, we speculated that the entry of infected DC into the PALS triggers antigen presentation to T cells. To test this hypothesis, we used Lm-specific CD8⁺ T cells from WP11.12 TCR transgenic mice (Mercado et al., 2000; Wong and Pamer, 2003) to detect antigen presentation in situ. BALB/c mice received 4×10^6 adoptively transferred CFSE-labeled WP11.12 CD8⁺ T cells and cells were allowed to home (4–8 hr) before mice were infected with Lm. At various times after infection, spleen cryosections were examined by immunofluorescence microscopy for T cell clustering as evidence of antigen recognition (Figure 4A). In the absence of infection (0 hr), WP11.12 T cells were distributed evenly in the PALS area and appeared bright and small, consistent with a resting phenotype. As early as 9 hr after infection, many WP11.12 T cells clustered in the PALS near the bridging channel (9 hr, inset), indicating that antigen presentation had begun. At 21 hr after infection, clusters had increased in size and moved into the center of the PALS, and by 41 hr, T cells had dissociated and large activated CFSE^lo WP11.12 T cells were distributed evenly through out the PALS (41 hr, inset). We could not detect WP11.12 T cell clusters in the MZ or RP over this time frame.

Infected CD11c⁺ cells were often associated closely with WP11.12 T cell clusters (Figure 4B, CD11c). These Lm-containing cells were MHC II⁺ and showed characteristic DC morphology (Figure 4B, MHCII). Although CD11b⁺ cells were found near T cell clusters, they were not MHC II⁺ and did not localize to the center of clusters (data not shown). Lm was typically observed in the center of T cell clusters in cryosections (Figure 4B) and in spleen explants via GFP-labeled bacteria and 2P microscopy (Figure 4C). We did not find T cell clusters associated with MARCO⁺ or MOMA-1⁺ macrophages during the first 41 hr of infection (data not shown). Thus, DCs appear to
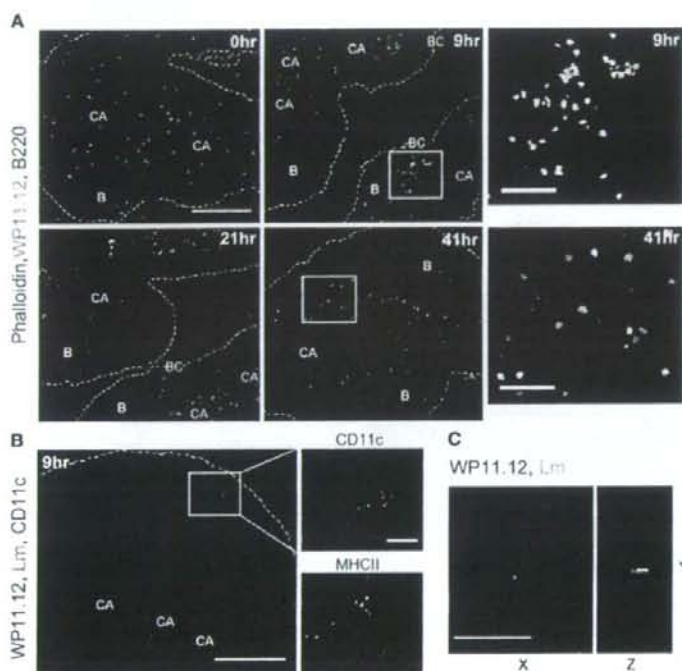
Figure 4. Antigen Presentation Kinetics and Location during Lm Infection in the Spleen

(A) CFSE-labeled WP11.12 CD8$^+$ T cells (4 × 10^6 cells, green) were adoptively transferred into mice before infection with 10^5 Lm. Spleens were harvested at the indicated times and stained with B220 to identify B cell follicles (red). White dashed lines indicate the edge of the white pulp based on phalloidin staining (blue). Scale bars represent 200 μm. Zoomed images (from white boxes) of WP11.12 cells in the PALS at 9 hr and 41 hr. Scale bars in zoomed images represent 50 μm. Figures are representative of more than five images per group from at least three independent experiments.

(B) Lm-specific T cell clusters (WP11.12, blue), CD11c$^+$ cells (red), and Lm (green) at 9 hr after infection. Scale bar represents 100 μm. Insets show zoomed in views of T cell clusters (blue) and CD11c or MHC II staining (red). Scale bar in zoomed image represents 20 μm. Images are representative of at least two independent experiments.

(C) 3D image of a representative Lm-specific T cell cluster (blue) ~10 hr after infection with 10^5 GFP-expressing Lm (cyan). BALB/c mice received 2 × 10^6 CMAC-labeled WP11.12 cells. Scale bar represents 20 μm.

be the primary APC type interacting with CD8$^+$ T cells in the early stages of infection.

Lm Transport to PALS Is Required for Antigen Presentation

We performed time-lapse 2P microscopy (Germain et al., 2006; Miller et al., 2002) to determine whether blocking Lm entry into the PALS with PTx would inhibit antigen presentation. Spleens were removed, secured to plastic coverslips with veterinary tissue adhesive, cut longitudinally with a vibrotome to expose the white pulp regions, and placed in warm oxygenated medium for imaging.
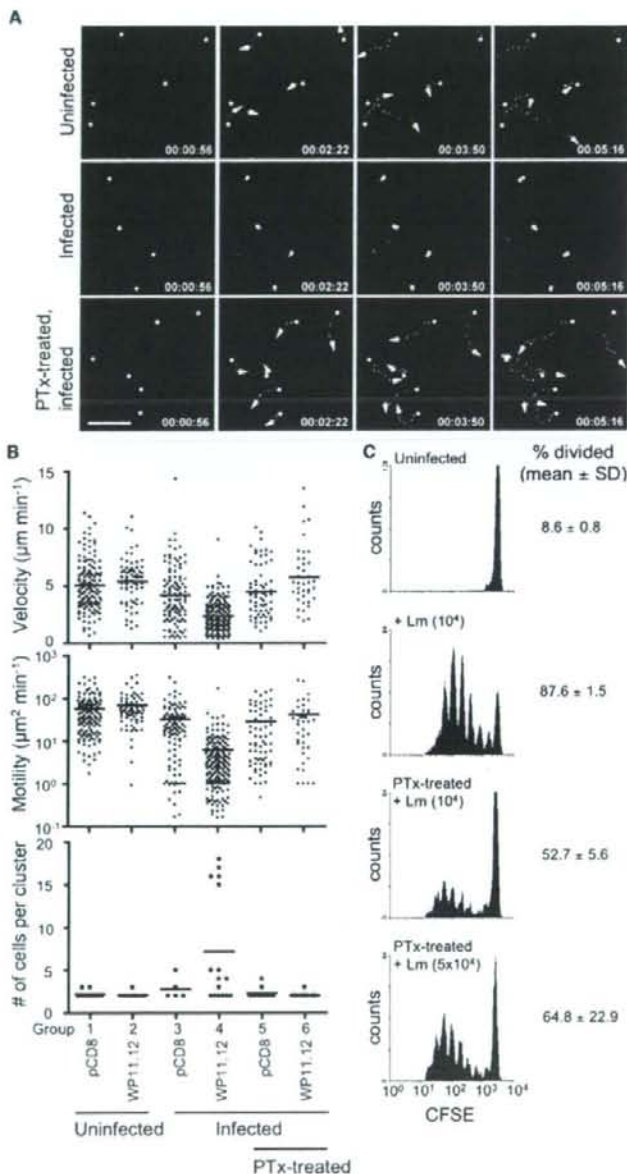
In uninfected mice, Lm-specific WP11.12 T cells moved randomly in the PALS with a median track velocity of ~5 μm min^{-1} and a motility coefficient of ~60 μm^{2}min^{-1}, similar to polyclonal CD8$^+$ T cells (Figures 5A and 5B; see also Movie S1). T cells migrated randomly and did not form clusters, similar to the T cell behavior previously observed in lymph nodes (Miller et al., 2002). However, the median T cell velocities measured in spleen explants were lower than mean values published for T cell migration in lymph nodes of ~12 μm/min (Miller et al., 2002). Our explanation for this discrepancy is that the decreased frame rate used in our current study (~2 images/min versus 4–6 images/min in previous studies) smoothes the characteristically large fluctuations in velocity associated with T cell motility and reduces the measured peak velocity in the data set. A decrease in peak velocity consequently yields a lower median velocity because the median is calculated from the velocity range. To investigate this issue further, we imaged T cells in explanted lymph nodes with our acquisition protocol and found slightly higher median T cell velocity (~7–8 μm/min, data not shown), suggesting that T cell motility is slightly slower in the spleen.

In infected mice, WP11.12 T cells showed significantly reduced velocity and motility (Figures 5A and 5B; see also Movie S2). Lm-specific T cells formed large aggregates in the PALS containing approximately 15 cells per cluster (Figures 4C and 5B). Occasionally, a few polyclonal CD8$^+$ T cells interacted transiently with the WP11.12 clusters, but most remained motile with no substantial reduction in velocity and motility (Figure 5B), indicating that cluster formation is antigen specific. Because the high antigen-specific T cell frequencies in adoptive transfer experiments can alter the kinetics and differentiation of responding T cells, we performed a limited number of experiments by using as few as 500,000 adoptively transferred Lm-specific T cells (Figure S6). Under these conditions we observed similar antigen recognition kinetics and clustering behavior (~4 cells per cluster; Figure S6; Movie S3).

When mice were pretreated with PTx to prevent Lm transport to the PALS, the clustering of bacteria-specific T cells was inhibited (Figures 5A and 5B; see also Movie S4). The lack of clustering was not due to the inhibition of T cell motility, because adoptively transferred polyclonal T cells moved with comparable velocity and motility in PTx-pretreated and untreated mice (Figures 5A and 5B) in our experimental protocol. When PTx was given ~2 hr after T cell adoptive transfer, we observed decreased T cell motility (data not shown), similar to the results of

A

B

C

Figure 5. PTx Inhibits Antigen Presentation to Lm-Specific CD8+ T Cells

(A) 2P time-lapse image sequences of T cells ~9 hr after infection in explanted spleens. Lm-specific WP11.12 T cells (4–6 × 10^6, blue) and polyclonal CD8+ T cells (5–7 × 10^6, red) were transferred into naive mice or PTx-pretreated mice. 6 hr later, mice were infected with 10^5 Lm. Representative WP11.12 cell tracks are shown (yellow lines). Scale bar represents 20 μm.

(B) WP11.12 and polyclonal CD8+ T cell (pCD8) tracks were analyzed for velocity, motility, and cluster formation. Bars show means for each data group (1–6). Data are representative of at least three independent experiments. Median velocity: group 1 versus 2, p > 0.05; 3 versus 4, p < 0.001; 5 versus 6, p > 0.05; 2 versus 4, p < 0.001; 2 versus 6, p > 0.05; 3 versus 5, p > 0.05; 4 versus 6, p < 0.001. Motility coefficient: group 1 versus 2, p > 0.05; 3 versus 4, p < 0.001; 5 versus 6, p > 0.05; 2 versus 4, p < 0.001; 2 versus 6, p < 0.05; 3 versus 5, p > 0.05; 4 versus 6, p < 0.001. Cluster size: group 1 versus 2, p > 0.05; 3 versus 4, p > 0.05; 5 versus 6, p > 0.05; 2 versus 4, p < 0.05; 2 versus 6, p > 0.05; 4 versus 6, p < 0.01. p values were calculated with the Kruskal-Wallis test.

(C) 5–7 × 10^6 CFSE-labeled WP11.12 T cells were adoptively transferred into mice. T cell proliferation was measured in uninfected control mice and on day 3 after infection in three experimental groups: mice infected with 10^4 Lm, mice pretreated with PTx then infected with 10^4 Lm, and mice pretreated with PTx and infected with 5 × 10^4 Lm (a five times higher dose was used in this group in order to compensate for the reduced Lm burden in the PTx-treated mice). PTx reproducibly inhibited Lm-specific T cell proliferation but did not completely block it. The mean ± SD of three mice in one representative experiment is shown. Data are representative of at least three independent experiments with similar results.

amined by 2P microscopy. Once Lm transport had occurred, PTx treatment no longer inhibited WP11.12 cluster formation whereas control T cells showed normal motility (Movie S5). Although Lm could be detected in the MZ and RP of PTx-treated mice (Figure 1D), we did not detect T cell clusters in these regions (Figure 4; 2P data not shown).

As a second indicator of antigen presentation, we measured adoptively transferred WP11.12 T cell proliferation by CFSE dilution assay. PTx pretreatment reproducibly decreased the number of proliferating WP11.12 T cells compared to untreated controls (Figure 5C). Decreased T cell proliferation was also observed when a larger inoculum of Lm was used to compensate for the lower Lm CFU present in PTx-treated mice at 24 hr (Figure 5C, bottom). We also assessed the ef-

others (Huang et al., 2007). This suggests that although PTx is capable of inhibiting T cell migration in the spleen, it does not remain active 24 hr after injection. As a further control for potential PTx effects on T cells, we administered PTx after Lm had entered the PALS (9–10 hr after infection). Lm-specific and polyclonal T cells were transferred and 2 hr later spleen explants were ex-

fects of PTx treatment on antigen presentation in vitro by using the Ova-specific OT1 transgenic T cells. DC were isolated from spleen and treated in vitro with 20 and 200 ng/ml Ptx for 2 hr (200 ng/ml is roughly equivalent to the in vivo dose of 500 ng per mouse.). After PTx treatment, DC were fed OVA or OVA-conjugated beads in the presence of LPS for 4 hr before coculture
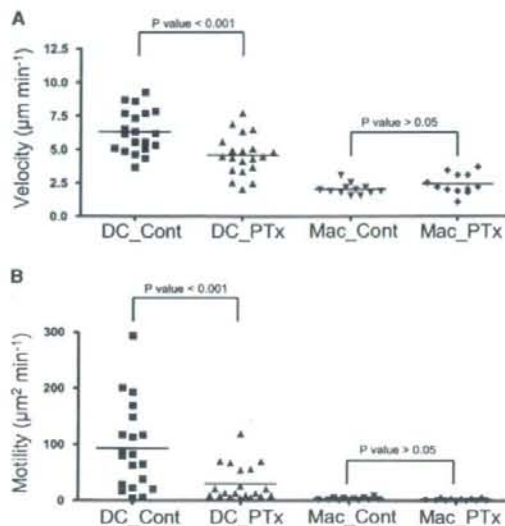
Figure 6. PTx Effects on DC and Macrophage Motility In Situ

Spleen explants were prepared (as described in Experimental Procedures) from CD11c-YFP mice (Lindquist et al., 2004) that received PBS or 500 ng of PTx 24 hr earlier. Spleen explants were imaged with 2P microscopy and cell motility analyzed (see Experimental Procedures for details).

(A) Median track velocity.

(B) Motility coefficient of DCs and macrophages (Mac) was determined. PTx significantly reduces DC motility and probing behavior but has no observable effect on macrophages, which are normally not motile in our time-lapse images. The data were generated from three independent experiments per group. One-way analysis of variance with Newman-Keuls Multiple Comparison post test was performed.

The p values for (A) are: Mac PTX versus DC_Control, p < 0.001; Mac_PTX versus DC_PTX, p < 0.001; Mac_PTX versus Mac_Control, p > 0.05; Mac_Control versus DC_Control, p < 0.001; Mac_Control versus DC_PTX, p < 0.001; DC_PTX versus DC_Control, p < 0.001. The p values for (B) are: Mac_PTX versus DC_Control, p < 0.001; Mac_PTX versus DC_PTX, p > 0.05; Marc_PTX versus Mac_Control, p > 0.05; Mac_Control versus DC_Control, p < 0.001; Mac_Control versus DC_PTX, p > 0.05; DC_PTX versus DC_Control, p < 0.001.

with OT1 T cells for 3 days. Ptx had no detectable effect on antigen presentation with either OVA or OVA-conjugated beads (Figure S7).

Next, we examined the effect of PTx treatment on the behavior of resident DCs and macrophages by using 2P microscopy. CD11c-YFP mice (Lindquist et al., 2004) were given a single i.p. injection of PTx (500 ng) 1 day before the spleens were harvested and prepared for time-lapse imaging. Fluorescent beads were injected i.v. to define the MZ and distinguish YFP+ MZMs (containing many beads) from DCs (containing few or none) in our analysis. In mock-treated mice, DCs showed active probing behavior and appeared to migrate randomly in the PALS and bridging channel with a median velocity of 6.3 μm/min (Movie S6 and Figure 6). We also observed DCs migrating to and from the MZ-PALS border. In Ptx-treated mice, DC probing behavior was lost and cell velocity was significantly reduced (p < 0.001,
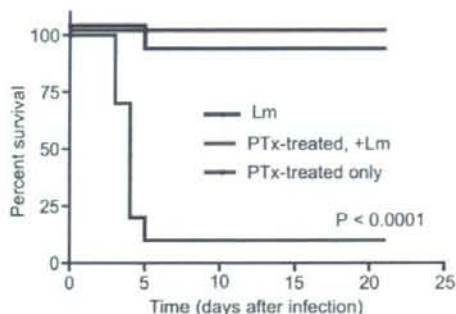
Figure 7. PTx Treatment Decreases the Survival of Mice after Lm Infection

Mice were pretreated with PTx i.p. then challenged with 5 × 10³ Lm EGD. Survival was followed for 21 days. p values were calculated with a log rank test (n = 10 mice per group). Black line, infected mice; red line, PTx-treated, infected mice; blue line, PTx-treated, uninfected mice. Ptx treatment severely compromised the host responses to Lm infection.

Movie S7 and Figure 6A). Although DCs were able to move slightly, they exhibited little displacement over time and their motility coefficient was significantly reduced (p < 0.001, Figure 6B). PTx treatment did not appear to alter the behavior of MZMs and these cells remained essentially nonmotile over the time frame of our imaging experiments (Movies S6 and S7 and Figure 6).

During sublethal Lm infection, T cell responses reduce the bacterial burden 5–7 days after challenge and over 2 weeks, resulting in the eradication of Lm. We tested whether blocking Lm entry to the PALS with PTx affected the survival of mice to primary infection. Although PTx-treated mice had reduced CFU in the spleen at 24 hr (Figure 1E), these mice could not control Lm at later times and succumbed to infection (Figure 7). Because endogenous lymphocytes are presumably exposed to PTx in these experiments, it is unclear whether PTx affects survival by inhibiting antigen presentation to CD8+ T cells or by inhibiting cell effector functions. Moreover, the decreased survival of PTx-treated mice could be due to the defective recruitment of TipDCs, which have been shown to be required to control Lm infection (Serbina et al., 2003).

DISCUSSION

In this study, we sought to determine whether DCs play a role in transporting bacteria from the MZ to the PALS, analogous to their role in carrying antigens from peripheral tissues to draining lymph nodes. The location and kinetics of bacterial antigen presentation in the spleen are poorly defined. 2P microscopy allowed us to assess antigen presentation in situ by quantifying changes in the motility and clustering of Lm-specific T cells. In the Lm infection model, we did not find evidence of bacteria-specific CD8+ T cell responses in either the MZ or RP during the first 2 days of infection, suggesting that the PALS is the primary compartment where CD8+ T cells first recognize antigen. In our study, we focused on the earliest detectable stages of antigen presentation. However, work with MHC class I tetramer staining in situ

showed that CD8^{+} T cells clustered at the T cell-B cell zone border and MZ beginning 3 days after infection (Khanna et al., 2007), suggesting that other regions of the spleen are involved at later times. Moreover, T cell responses were detected in the splenic RP after an i.v. injection of soluble peptide (Odoardi et al., 2007), demonstrating that antigen presentation can occur outside the PALS. To what extent immune responses to viruses and other bacteria are initiated in distinct splenic compartments is an interesting question. If the location of antigen presentation is dependent on the type and route of infection, then the tissue microenvironment where antigen presentation occurs might play a pivotal role in shaping the character of the pathogen-specific immune response.

Our primary evidence linking Lm transport to antigen presentation is that PTx treatment inhibits both the entry of bacteria into the PALS and the recognition of bacterial antigen. We used 2P imaging to analyze Lm-specific T cell responses and found that PTx inhibited the clustering and arrest of T cells only if administered before Lm gained entry into the PALS. We found that PTx treatment after T cell adoptive transfer does indeed decrease T cell velocity in the spleen, as observed by others (Huang et al., 2007; Okada and Cyster, 2007). However, in our protocol, the inhibition of antigen presentation by PTx is due to blocking APC migration and not due to inhibition of T cell motility, because adoptively transferred T cells appear unaffected (i.e., motility was identical in PTx-treated and untreated mice). Moreover, when we gave PTx 2 hr before T cell transfer, control T cells showed normal motility and Lm-specific T cells clustered normally. Our explanation is that PTx is rapidly consumed in vivo and does not affect T cells transferred subsequently.

Our 2P microscopy experiments revealed that PTx markedly inhibited DC motility in the spleen. Previously, PTx was reported to inhibit DC homing to the thymus, but not the spleen (Bonasio et al., 2006). Although DCs may enter the spleen passively from the circulation, DC migration into the PALS appears to require chemokine receptor signaling, as suggested by studies with CCR7-deficient knockout mice (Kursar et al., 2005).

There were no statistical differences in CFU counts per spleen between Ptx-treated mice and untreated controls during the first 6 hr of infection, suggesting that PTx treatment did not interfere with the initial trapping of Lm. However, the increased CFUs in PTx-treated mice at 24 hr indicated that the infection does not progress normally and that Lm proliferation in the PALS is inhibited. Although PTx could interfere with actin rearrangements involved in the host cell invasion by Lm or cell-cell spread, we believe that the main effect of PTx is on splenocyte migration because others have shown that ActA-deficient Lm were capable of invading and proliferating in the PALS, albeit at a lower level (Muraille et al., 2005). Moreover, we performed histological experiments to examine the impact of PTx pretreatment on Lm capture and found that the cellular distribution and amount of bacteria captured was similar to untreated control mice.

Neuenhahn et al. (2006) concluded that viable Lm was found exclusively in CD8α[+] DCs 3 hr after infection and proposed that these DCs were responsible for the initial trapping of live Lm in the spleen. Our results extend on previous work by showing that DCs facilitate Lm entry into the PALS and that this entry is required for efficient antigen presentation. It is noteworthy that we found infected MOMA-1^{+} macrophages and CD11b^{+} cells

in the PALS at 24 hr, but did not find CD8^{+} T cell clusters associated with these cells, and therefore their role in antigen presentation remains unclear. A variety of splenic phagocytes capture Lm initially, but bacteria expand transiently in DCs, suggesting that DCs may support Lm growth in vivo (unpublished observations). It is possible that the transient proliferation of bacteria in DCs is advantageous to host survival because it would be expected to provide abundant cytosolic antigen to stimulate CD8^{+} T cell-mediated immunity.

The role of different DC subsets in Lm pathogenesis and antigen presentation is a key question that is difficult to address because current methods for DC ablation, such as the CD11c-DTR system, deplete all CD11c^{+} DCs, as well as splenic macrophages (Probst et al., 2005). The spleen contains two main DCs subsets, CD8α^{+}DEC205^{+} DCs, which reside in the PALS and bridging channel (Steinman et al., 1997) and present MHC I bound peptides more efficiently (Dudziak et al., 2007), and CD8α^{−}, 33D1^{+} DCs found primarily in the RP and MZ (Steinman et al., 1997), which present antigen to CD4^{+} T cells preferentially. Neuenhahn et al. (2006) observed CD8α^{+} DCs in the MZ and RP where they would have direct contact with Lm entering the spleen. Although CD8α[+] DCs were shown to preferentially contain live Lm, DCs were not strictly required for antigen presentation because the adoptive transfer of infected macrophages could restore T cell responses in mice depleted of DCs (Neuenhahn et al., 2006). CD8α[+] DC have been shown to prime T cell responses to Lm (Belz et al., 2005), suggesting that these DCs play a central role in stimulating Lm-specific responses. Moreover, CD8α[+] DCs are specialized for crosspresentation (den Haan et al., 2000) and this function may be important for stimulating T cell responses to Lm. In our study it is noteworthy that we often found T cell clusters around infected DCs, suggesting that early CD8^{+} T cell activation proceeds primarily via the classical MHC I pathway. We did not examine MHC II antigen presentation and it is entirely possible that different regions of the spleen and distinct APCs might be involved in activating CD4^{+} T cells (Odoardi et al., 2007).

Defining the precise cellular mechanisims that deliver bacterial antigens to the PALS is important for understanding how antigen presentation occurs in the spleen. Recently, Cinamon et al. (2008) showed that MZ B cells shuttle soluble antigen from the MZ to follicles in the white pulp in a CXCR5-dependent manner. Because the entry of Lm into the PALS is sensitive to PTx treatment, bacterial transport likely involves chemokine signaling as well. CCR7-deficient mice showed decreased T cell priming and increased susceptibility to Lm infection (Kursar et al., 2005). This result was attributed to the failure of T cells and DCs to efficiently colocalize in the absence of CCR7; however, this study did not address the impact of CCR7 deficiency on Lm transport and antigen presentation directly. The work of others suggests that the transport of Lm to the PALS is contingent on the cytosolic entry of bacteria given that neither heat-killed nor LLO-deficient Lm enter the host cell cytosol and both fail to reach the PALS after i.v. challenge (Glomski et al., 2003; Lauvau et al., 2001; Muraille et al., 2005). Importantly, these noncytosolic forms of Lm also fail to elicit robust T cell immunity, suggesting a link between PALS infection and T cell priming. As suggested by Muraille et al. (2005), a critical step in the progression of Lm infection to the PALS might be the recognition

of bacteria by intracellular sensors such as the NOD-like receptors (Mariathasan and Monack, 2007; Dufner et al., 2007; Park et al., 2007).

There are several plausible mechanisms for Lm entry to the PALS: migration of infected DCs from MZ to PALS, migration of PALS DCs to the MZ boundary to capture and carry back Lm, and cell-cell spread of Lm from MZ to PALS. The issue of cell-cell spread has been addressed by experiments with ActA-deficient Lm, which cannot mobilize host cell actin (Muraille et al., 2005). In the presence of gentamicin, ActA-deficient Lm can still enter the PALS, arguing that PALS infection does not require cell-cell spread. Ideally, single-cell tracking experiments with GFP-Lm and 2P microscopy will help determine whether one or more of these mechanisms is at work.

We propose that early host-pathogen interactions in the MZ lead to the transport of intracellular antigen to the PALS for presentation to T cells. Our results with Lm suggest that targeting antigen delivery to the PALS might be an effective strategy to enhance vaccine efficacy and the priming of CD8^{+} T cells to intracellular pathogens.

EXPERIMENTAL PROCEDURES

Mice

BALB/cJ mice were obtained from The Jackson Laboratory. CD11c-YFP mice (Lindquist et al., 2004) were a gift from the M. Nussenzweig lab. WP11.12 TCR transgenic mice, expressing a transgenic TCR that recognizes p60$_{449-457}$ peptide in the context of H-2K^d (Mercado et al., 2000), were a gift from E. Pamer (Sloan-Kettering Institute, NY). Mice were maintained and bred under SPF conditions in the Washington University mouse facility.

Bacteria, Fluorescent Beads, and Dextran

The GFP-expressing Lm EGD strain was made with the pNF8 vector (Fortinea et al., 2000). The LD$_{50}$ of our GFP-expressing Lm strain was 1.1×10^5 in BALB/c mice, or ~50-fold attenuated compared with wild-type EGD. Both GFP-expressing Lm and the EGD strain were stored as frozen glycerol stocks (~1 × 10^9/ml) at −80°C. Mice were infected with Lm diluted in PBS (to indicated doses) from frozen stocks or overnight cultures. For infection times less than or equal to 2 hr, we typically used 10^7 EGD Lm. For infections at 12 and 24 hr, we used 10^4–10^5 bacteria. FluoSpheres carboxylate-modified microspheres (yellow-green, 1.0 μm and 0.5 μm) and Fluorescein-conjugated dextran (lysine-fixable, 500 kD) were purchased from Invitrogen. All reagents were injected i.v. in a volume of 200 μl.

Histology

Mice were euthanized and spleens harvested and embedded in Tissue-Tek OCT compound. 5 μm cryosections were cut and fixed with 4% paraformaldehyde in PBS (pH 7.2) at 4°C for 5 min and then blocked with StartingBlock Blocking Buffer (PIERCE) for 10 min before being sequentially incubated with fluorescent dye-conjugated or biotin-conjugated primary antibodies (1:100 dilution with blocking buffer), fluorescent dye-conjugated secondary antibodies and/or fluorescent dye-conjugated streptavidin (1:100 dilution with blocking buffer). Sections were mounted in GVA mount (Invitrogen) and stored at 4°C. Details for antibodies and reagents used for immunofluorescence staining can be found in the Supplemental Data.

Immunofluorescence Microscopy

Four-color fluorescence microscopy of cryosections was performed with an Olympus BX51 equipped with 100W mercury lamp (Olympus) and a SPOT RT CCD camera (Diagnostic Instruments). Monochrome images (1200 pix × 1600 pix = 885 × 1180 μm with 10× objective; 440 × 586 μm with 20× objective, 12-bit depth) were acquired through fluorescence filters optimized for DAPI, FITC, TRITC, and Cy5 (Chroma). Images were acquired, processed to reduce background, pseudo-colored, and merged with SPOT RT camera soft-

ware. Immunofluorescence images were segmented into splenic compartments and the number of pixels specific for Lm staining or fluorescent beads was measured and expressed as the percentage of pixels in each compartment (see Supplemental Data for details).

Pertussis Toxin and Clodronate Liposome Treatment

PTx was purchased from Sigma (St. Louis, MO). Mice were injected with 500 ng of PTx i.p. 1 day prior to infection (10^7 for 0.5 hr and 10^5 for 24 hr) and Lm tissue distribution was assessed by immunofluorescence at 0.5 and 24 hr later. In other experiments, the survival of PTx-treated mice after Lm infection with 10^3 CFU of EGD (LD$_{50}$ ~2 × 10^3 in BALB/C mice) was determined. In 2P experiments, mice were given 500 ng PTx i.p. 1 day before to the transfer of fluorescently labeled Lm-specific and polyclonal T cells. T cells were allowed to home for several hours and then mice were infected by an i.v. injection of Lm (10^4 for EGD or 10^5 GFP-Lm). Approximately 9 hr later, spleen explants were cut and imaged with 2P microscopy and T cell behaviors (velocity and clustering) analyzed. In some experiments, PTx was administered 8–9 hr after infection to allow Lm time to enter the PALS. T cells were adoptively transferred 1–2 hr later and T cell behaviors analyzed with 2P microscopy for changes in motility and clustering beginning at ~2 hr after T cell transfer.

For depletion of phagocytes, clodronate liposome suspensions were prepared as described previously (Calderon et al., 2006; van Rooijen and van Kesteren-Hendrikx, 2003). Mice were given 200 μl of clodronate liposome suspension i.v. 2 or 6 days before infection. The depletion of macrophages and dendritic cells was assessed on day 2 and day 6 by staining sections for MARCO, MOMA-1, CD11b, and CD11c. Spleens were examined by immunofluorescence microscopy 24 hr after infection to quantify the amount of Lm in the MZ, RP, and PALS regions. Similar depletion and recovery experiments were preformed with the CD11c-DTR system of Jung et al. (Jung et al., 2002; Probst et al., 2005).

Two-Photon Microscopy

CD8^{+} T cells were purified by negative selection with magnetic beads (Miltenyi Biotec) from BALB/cJ or WP11.12 mice (Mercado et al., 2000), then labeled for 30 min at 37°C with 20–50 μM CMAC, 10 μM CFSE, or 10 μM CMTMR (Invitrogen). T cells (5 × 10^5–7 × 10^6) were resuspended in 200 μl of PBS, adoptively transferred by tail vein injection and allowed to home for several hours before mice were infected with 10^5 EGD Lm. In some experiments, we infected mice with 10^6 GFP-expressing Lm to localize bacteria and T cell clusters in 3D space. Explanted spleens were secured to coverslips with a thin film of VetBond (3M). To image the WP, spleens were cut longitudinally with a vibratome (Pelco). Spleen sections were placed in a flow chamber and maintained at 37°C by perfusion with warm, high-glucose DMEM bubbled with a mixture of 95% O$_2$ and 5% CO$_2$. Time-lapse imaging was performed with a custom-built two-photon microscope, fitted with two Chameleon Ti:sapphire lasers (Coherent) and an Olympus XLUMPlanFl 20× objective (water immersed; numerical aperture, 0.95) and controlled and acquired with ImageWarp (A&B software). For imaging of GFP, the excitation wavelength was 890–915 nm; for CMTMR and CMAC, 780–800 nm was used. Signals from fluorescent dyes and GFP were separated by dichroic mirrors (490 nm, 515 nm, and 560 nm). To create time-lapse sequences, we typically scanned volumes of tissue 100 × 120 × 75 μm with 31 Z-steps of 2.5 μm each at 30–45 s intervals for up to 60 min.

CFSE T Cell Proliferation Assay

Purified 5–7 × 10^6 WP11.12 T cells were labeled with CFSE (5 μM) and transferred to recipient mice 2 hr before Lm infection (10^4). PTx-treated mice were given 500 ng of PTx i.p. 24 hr prior to infection with Lm (10^4 and 5 × 10^4). Beginning at 24 hr after infection, mice were given ampicillin (5 mg/ml in drinking water) to eliminate bacteria. On day 3 of infection, CFSE dilution was assessed by flow cytometry (2 × 10^6 cells) with Vβ8.1 to enrich for WP11.12 T cells in the analysis.

Data Analysis

Cells were detected based on fluorescence intensity and cell tracks obtained with Volocity (Improvision) or Imaris (Bitplane) software. Tracks greater than 3 min (≥7 time points) were included in the analysis. Cell velocities were reported as the median of instantaneous velocities in each cell track. Motility